

FPDETECT: Efficient Reasoning About Stencil Programs Using Selective Direct Evaluation

ARNAB DAS, University of Utah

SRIRAM KRISHNAMOORTHY, Pacific Northwest National Laboratory

IAN BRIGGS, University of Utah

GANESH GOPALAKRISHNAN, University of Utah

RAMAKRISHNA TIPIREDDY, Pacific Northwest National Laboratory

We present FPDETECT, a low overhead approach for detecting logical errors and soft errors affecting stencil computations without generating false positives. We develop an offline analysis that tightly estimates the number of floating-point bits preserved across stencil applications. This estimate rigorously bounds the values expected in the data space of the computation. Violations of this bound can be attributed with certainty to errors. FPDETECT helps synthesize error detectors customized for user-specified levels of accuracy and coverage. FPDETECT also enables overhead reduction techniques based on deploying these detectors coarsely in space and time. Experimental evaluations demonstrate the practicality of our approach.

1 INTRODUCTION

Approaching the end of Moore's law, chip manufacturers are seeking smaller lithographies, higher densities often achieved by emerging 3D stacking methods, newer memory/interconnect technologies, and increasing use of GPUs and other accelerators. These trends are increasing the likelihood of soft errors [4, 9, 37, 40, 42] already noticed to be high in GPU-based systems [49]. The increased pressure toward specialization [26] may reduce the economies of scale achieved through general purpose parts, and put cost-reduction pressures on verification methods, which already are stressed [29]. This can increase residual logical bugs in chips. The increasing complexity of compiler optimizations will also increase the likelihood of introducing logical bugs [3]. Software-level error detectors can serve as uniform and application-aware ways of trapping both soft errors [38] and logical bugs [3], and these detectors are needed more than ever before.

Unfortunately, system resilience research has, so far, gone nowhere in terms of adoptions into practice. The main underlying reason is that in today's systems, these resilience solutions geared toward soft errors will largely cause a slowdown, with no apparent benefits from the point of view of soft errors. It may even aggravate the problem due to the high false positive rates in today's resilience solutions. Last but not least, today's resilience solutions have not been demonstrated to have the ability to reliably flag logical errors.

Our main contribution in this paper is to demonstrate that for a narrow class of applications—specifically stencil-based—we can indeed develop solutions that benefit *both* logical error protection and soft error protection, owing to our solutions having two key attributes: (1) no false positives, and (2) acceptable overheads. With this combination, we strongly believe that resilience solutions will be welcomed more readily, at least for their immediate impact on logical bugs.

Stencils belong to an important class of iterative solvers operating on dense D-dimensional arrays modeling partial differential equations (PDEs) with applications belonging to fluid dynamics,

New paper, not an extension of a conference paper.

2019. XXXX-XXXX/2019/11-ART1 \$15.00

<https://doi.org/>

cosmology, combustion, etc.¹ They are part of the essential building blocks for solving larger more composite problems involving multiple PDEs.

The ability to write good assertions that capture a stencil computation’s evolving profile of data is tricky and error-prone. Existing work on system resilience that address data integrity include time-series data analysis methods [17] and data outlier detection methods constructed using machine learning (e.g. [44, 46]). Unfortunately, these approaches have high overheads, and can only help loosely characterize the expected data value ranges. They additionally bring in training bias into the models constructed. Given that they both overestimate and underestimate the data ranges, detectors based on them generate both false positives and false negatives. With soft error detection, false positives are virtually unacceptable, given that the natural soft error rates themselves are quite low (false positive needlessly engage checkpoint/recovery systems).

FPDETECT is the first approach that takes the novel approach of basing data-space protection on *accurate floating-point round-off error estimation*. Like any calculation carried out by numerical code, stencil-based calculations are also subject to floating-point rounding error. However, given that stencils are more structured, we show that one can develop a rigorous floating-point round-off error estimation approach for them, guaranteeing a certain number of mantissa bits after every stencil application. Consequently, in the FPDETECT approach, if “round-off” appears suddenly exaggerated, we can attribute it reliably—without any false positives—to a logical bug or a soft error.

Contemporary floating-point error estimation approaches using interval analysis [6, 32] tend to give excessively conservative estimates (due to loss of correlation) of round-off error—especially for large programs that are iterated over time. These conservative estimates with large error bounds implies guarantees for only the higher order mantissa bits, i.e., only those errors that cause very high magnitude changes can be trapped using them.² FPTaylor [12] builds symbolic taylor forms for the error expressions resulting in tight guarantees but do not scale to be usable beyond a few hundred operators. FPDETECT on the other hand provide tighter guarantees on the error for large stencil programs, thus helping protect more mantissa bits, and also allows a *tunable* approach to trading off overhead against detection precision, as we show in this paper.

Classical approaches like dual modular redundancy (DMR) can rigorously detect silent data corruptions by utilizing a duplicated execution thread and checking for result matches. This unfortunately can double the overall computation time. Clover [33] exercises a selective instruction duplication strategy to bring down the SDC detection cost to around 26% using tail-DMR. However, this approach is meant only for soft errors; it cannot be used to trap compiler bugs because they impact *both* the execution threads.

In this paper, we show that by focusing on a narrow (but important) class of applications—in our case stencils—we can arrive at a *unified solution* for detecting compiler bugs and soft errors while also offering rigorous guarantees. We offer our tool FPDETECT, a *software based error detector*, whose core approach is based on rigorous floating-point round-off error analysis for an iterated application of the stencil across T computational steps. To the best of our knowledge, this is the first work that encompasses two important correctness checks around the single central idea of offline round-off analysis.

ROADMAP: §2 provides an overview of FPDETECT including error analysis, and optimizations. §3 is an overview of how FPDETECT helps detect software bugs and soft errors. To reduce overheads, we establish a crucial result that if we leapfrog stencil applications and the detectors T steps ahead do not detect a soft error, then we can establish a *certified baseline* that allows earlier time steps to be forgotten based on the fact that uncaught soft errors in earlier steps will not affect future detection.

¹While our approach applies to sparse stencils, we focus on stencils operating on dense matrices.

²That is, should these methods be used to synthesize error detectors, which hasn’t been done.

This allows FPDETECT detectors to be deployed sparsely in space and time (e.g., once per 64 time steps) (§4 and §5). We perform offline detector synthesis to create lookup tables, and instantiate specific detectors just before execution (§6). Our evaluation (§7) includes results on software bug detection and resilience (both simulated through fault injection). Additional related work (§8) and conclusions (§9) follow.

2 OVERVIEW

Background on Floating-point error analysis: Floating-point error analysis is a vast area, and we provide only a brief overview (see [24, 36] for details). A floating point number system, \mathbb{F} , in radix, β , is a subset of the set of real numbers, and can be expressed as a 5 tuple (β, s, m, e, p) . We use binary ($\beta = 2$) double precision with number of *precision bits*, $p = 53$. $s \in \{-1, 1\}$ is the sign bit, e is the exponent in the range $-1022 \leq e \leq 1023$, and m is the mantissa or the significand, and represents the magnitude $s \cdot m \cdot 2^e$. If $x \in \mathbb{R}$, then $x_f \in \mathbb{F}$ denotes an element in \mathbb{F} closest to x obtained by applying the rounding operator (\circ) to x . We use the bound consistent for all IEE754 [1] rounding modes.

In floating point arithmetic, the *absolute error* is the magnitude difference between the values yielded by computations done in the space of real numbers (“true answer”) and those done in floating point. The relative error is the ratio of the absolute error and the true answer. Every real number x lying in the range of \mathbb{F} can be approximated by an element $x_f \in \mathbb{F}$ with a relative error no larger than the *unit round-off* $\mathbf{u} = 0.5 \times \beta^{1-p}$. Here β^{1-p} corresponds to the *unit of least precision (ulp)* for exponent value of 1. We use μ to denote $\text{ulp}(1)$, such that $\mu = 2\mathbf{u}$. In our case $\mathbf{u} = 2^{-53}$, and hence $\mu = 2^{-52}$. Hence, for all rounding modes(\circ), $\circ(x) = x(1 + \delta)$, $|\delta| \leq \mathbf{u} = \mu/2$. Given two exactly represented floating point numbers x_f and y_f , arithmetic operators $\diamond \in \{+, -, \times\}$ have the following guarantees across any rounding modes:

$$x_f \diamond_f y_f = (x_f \diamond y_f)(1 + \delta) = (x_f \diamond y_f) + (x_f \diamond y_f)\delta, \quad |\delta| \leq 2\mathbf{u} = \mu \quad (1)$$

In our work, we employ affine arithmetic [16] for error estimation. In an affine representation, each input variable \hat{x} is represented by $\hat{x} = x_0 + \sum_{i=1}^n x_i \epsilon_i$, with x_0 denoting the central value of the corresponding interval, and coefficients x_i being finite floating point numbers. The ϵ_i are *formal noise variables* which are unknown until concretized but assumed to lie in the interval $[-1, +1]$. The x_i model the noise coefficients such that the round-off error in equation (1) can be expressed as $x_i = (x_f \diamond y_f) \times 2$, with a noise variable $\epsilon_i \in [-1, 1]$.

We define two operators, σ and γ that allows us to retrieve the associated noise variable and coefficient information for each affine variable.

- σ : Defines the mapping from an affine variable to its set of noise variables. Thus $\sigma(\hat{x}) = \{\epsilon_i\}_{i=1}^n$.
- γ : Defines the mapping from a 2-tuple of (*affine variable, noise variable*) to its corresponding noise coefficient. Thus $\gamma(\hat{x}, \epsilon_i)$ return x_i if $\epsilon_i \in \sigma(\hat{x})$ else return 0.

Using these operators, at every operator site, a fresh noise variable is introduced and their collective impact in the forward path is tracked using affine analysis. For codes implemented with the round to nearest model (as in most cases), one can configure $\mathbf{u} = \mu$, to obtain stricter bounds.³

Illustrative example: We now illustrate the concepts and practical details behind FPDETECT using the simplified 1D stencil of 3 inputs leapfrogged (iterated) over 6 time steps (Figure 1). In this example, the stencil coefficients are 0.25, 0.5, 0.25 (say, modeling discretized heat flow) working on problem array A . The value $A[x, t + 1]$ can be calculated to be $0.25 * A[x - 1, t] + 0.5 * A[x, t] + 0.25 * A[x + 1, t]$. We call this approach of obtaining the values at the next time step the *iterated* evaluation scheme.

³A full derivation of error bound using affine arithmetic are presented in the separate **supplementary material** for the interested reader in **Appendix A**

Table 1. Evolution of Coefficient values as we unroll the stencil

Set Number	Coefficients at Offsets						
offset index \rightarrow	-3	-2	-1	0	1	2	3
Set_1	0	0	0.25	0.5	0.25	0	0
Set_2	0	0.0625	0.25	0.375	0.25	0.0625	0
Set_3	0.015625	0.09375	0.234375	0.3125	0.234375	0.09375	0.015625

One can also imagine obtaining the value at $A[x, t + 6]$ through *direct* evaluation that leapfrogs 6 steps, provided one calculates the *effective path coefficients*. Table 1 illustrates how these coefficients may be calculated by taking the sum of the product of the path weights (Set_2 , for instance, is $0.375 = 0.25 * 0.25 + 0.25 * 0.25 + 0.5 * 0.5$).

Now, given a specific unroll (leapfrog distance) of T , we can then generate a similar table for that unroll, obtaining, for a k point stencil, $(k - 1)T + 1$ effective coefficients. For example for a 3-point stencil over $T = 5$ steps, we obtain 11 separate coefficients for contribution from each of the corresponding unrolled points. Then, given $(k - 1)T + 1$ runtime values of these points, the direct evaluation scheme can obtain the value T steps ahead, and is the basis of realizing FPDETECT detectors. We in fact implement this dot product of input values with the effective coefficients being in higher precision, and also employ Kahan’s [30] summation algorithm, as well as vectorization, thus minimizing the *relative error* of this answer.⁴ Thus we obtain an estimate for the relative error with minimal precision loss; call it R_d for *relative error under direct evaluation*.

While we know R_d , we cannot give any bounds on the number of mantissa bits preserved unless we also know the iterated evaluation’s relative error, say R_s (s for “serial” evaluation). A key contribution we make is to tightly estimate R_s analytically.

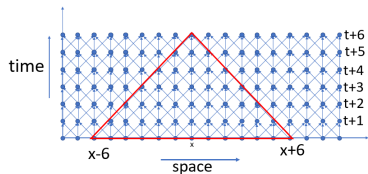


Fig. 1. Simplified 1D stencil over 6 time steps

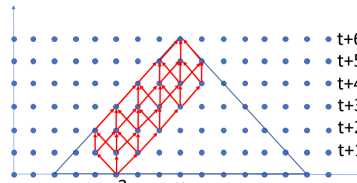
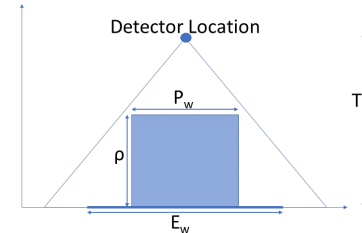


Fig. 2. Illustration of path dominance

Fig. 3. Essential (E_w) and protected widths (P_w)

Iterated Evaluation: That there are many reconvergent computational paths to be taken into account during iterated evaluation for generating the output at $[x, t + 6]$ from the inputs at t . In such situations, unless we keep the errors on various re-convergent paths correlated, we will obtain uselessly exaggerated error bounds. Fortunately, affine arithmetic is well known for being able to handle error analysis in such situations. As an example, $(x - x)$ yields 0 under affine arithmetic (whereas interval arithmetic will yield an interval with the error in x doubled [36]).

FPDETECT comprises of an offline phase which includes static error analysis of the stencil combined with conservative profiling of the stencil (detailed in 6) for a set of protection goals as shown in Figure 6. Our error analysis method uses affine arithmetic building upon the works of [6, 13, 27] but are applied to much larger expressions. As a simple illustration, consider a single step iteration of a 1-d 3-point stencil with stencil coefficients $\{c_1, c_2, c_3\}$ centered around x_2 to evaluate x_2 for the next time step, denoted here as S in Figure 4. Thus the computational graph

⁴We also employ vectorization to reduce overheads in the FPDETECT detector.

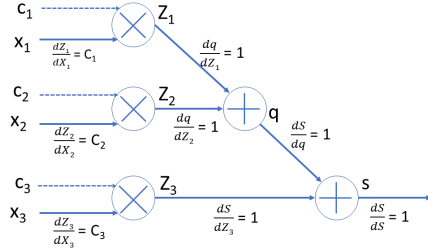


Fig. 4. Computational graph with highlighted derivatives for 1 step of a 1-d 3-point stencil

evaluates $S = ((c_1 \times x_1) + (c_2 \times x_2)) + (c_3 \times x_3)$. If ϵ' is a noise variable belonging to $\sigma(x_1)$, then the error contribution's propagation at S will be

$$\begin{aligned} \gamma(x_1, \epsilon') \cdot K_{x_1} &= \gamma(x_1, \epsilon') \cdot \left| \frac{dS}{dx_1} \right| = \gamma(x_1, \epsilon') \cdot \left| \frac{dS}{dS} \cdot \frac{dS}{dq} \cdot \frac{dq}{dz_1} \cdot \frac{dz_1}{dx_1} \right| = \gamma(x_1, \epsilon') \cdot 1 \cdot 1 \cdot 1 \cdot c_1 \\ &= \gamma(x_1, \epsilon') \cdot c_1 \end{aligned} \quad (2)$$

Thus for all such $\epsilon' \in \sigma(x_1)$, the $\gamma(x_1, \epsilon')$ gets propagated by c_1 (and similarly for x_2, x_3, z_1, z_2, z_3 and q). Effectively, every incoming node or an internal compute node has a locally generated error term, and a propagation factor that propagates this error to the output node.

We can iteratively evaluate the stencil and arrive at this output value by (conceptually) picking all intermediate points, such as P that is highlighted in Figure 5, and first finding the error flowing into P . Then find out how this error is *modified* by all the path coefficients from P to the output. Do this for each point in the iteration space that iteratively contribute to the output at the detector location. Accumulating these error terms and normalizing them gives us the relative error R_s under iterated evaluation. While iterated evaluation mimics the stencil evaluation itself, *we are conservatively estimating this error during the offline phase* of FPDETECT. Our error analysis suitably combines the error for all such conceptual points P using affine arithmetic.

Detector precision (dp_T): We now can define a precision threshold to be checked for correctness at the detector locations.⁵ Called *detector precision* dp_T (where the subscript T indicates it is a function of the number of lookahead Tsteps) it is defined as $\text{bits preserved}_T = (dp)_T = p - \log_2(\max(R_s, R_d))$ which says “remove the maximum of the uncertainties between the direct and iterated evaluations.” Given that we minimize R_d , the key factor impacting the number of bits preserved will be the main stencil's iterated evaluations. Soft errors or logical bugs that throw the actual error beyond the dp_T limit can then be trapped with the guarantee of *no false positives*. Furthermore, all events whose impact falls within the guaranteed precision will be trapped. The only case of omission (which is outside of our model) is when two faults simultaneously land within the scope of two adjacent detectors, and both these fault-flows cancel out before reaching their respective detectors.

Offline/Online Split: Our approach consists of an offline phase and an online one (Figure 6). The user presents the uninitialized input stencil and the range of intervals (in binades—meaning exponent spans) expected for each input. In the offline phase we explore a rich search space. It is composed of the exponent binade ranges, and protection goals defined by required precision accuracy and protection coverage. The goal is to obtain a best fit detector configuration for a pair of (*precision, coverage*) for each exponent binade and populate a look-up table for each application. Each application is identified by its unique coefficient set. Note that any change of coefficients for a

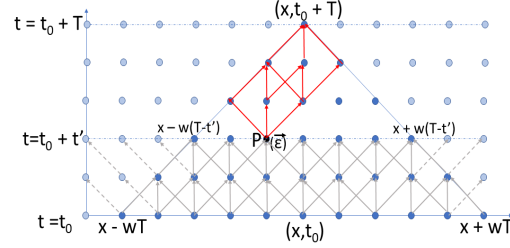


Fig. 5. Error propagation from point $(x-1, t_0+t')$ to (x, t_0+T) (1-d stencil)

⁵A full derivation of dp_T including affine arithmetic and error analysis details are presented in the separate **supplementary material** for the interested reader in **Appendix A**.

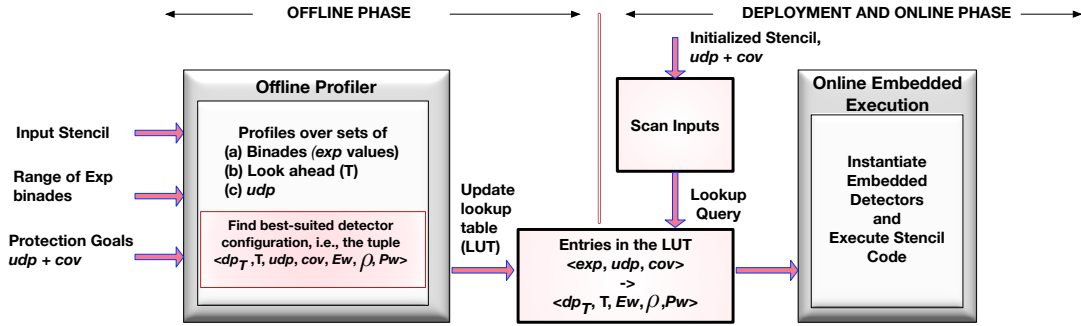


Fig. 6. Overview of FPDETECT

given stencil results in re-synthesis as a new application, creating a new entry in the lookup table. In online phase, we scan the input to obtain an interval that maps to a canonical exponent binade range. This allows FPDETECT to query the LUT for any unseen data at runtime with user defined precision and coverage goals to obtain a best fit detector configuration. Given these inputs, we can calculate *the worst-case binade differences* present at the input. The binade difference influences R_s and R_d : the higher the worst-case binade differences at the input, the worse R_s and R_d themselves are, and the lower the value of dp_T . The goal of the offline phase is to produce a *look-up table* (LUT) which has the guarantee of dp_T bits at the detector output, provided the runtime data lives within the binade differences upon which the stencil is “profiled.” The worst case binade difference is extracted only at the beginning for the initialized input set in our experiments. Our rigorous guarantees are with respect to these binade differences (a fact that can be optionally revalidated at runtime).

Protected Width: Our runtime goal is to not deploy the detectors at every time step, but only at every ρ time steps (Figure 3, where x-axis corresponds to the grid points in the stencil evaluation) by certifying the correctness of points within the ρ detection latency. Moreover, our goal is also to spatially distribute the detectors sparsely: the $\rho \times P_w$ boxes shown in this figure capture this goal, and these boxes are stacked horizontally. To arrive at these “stacking” optimizations, the user also provides the protection goals (*user defined precision* or udp defined in §4). Then during the online phase, we can provide udp number of bits to be preserved in the computational volume presented in each $\rho \times P_w$ box, provided dp_T bits are guaranteed by the detector.

The actual stencil computation and detector deployment in a realistic problem are as presented in Table 2. In particular, FPDETECT can handle multiple computational arrays that iteratively update each other over time. With respect to the parameters specified in Table 2, FPDETECT automatically instantiates and configures the requisite detectors. The pseudo-code in Figure 7 also presents the automatically inserted DETECT_ERRORS() calls corresponding to where the error is detected.

Figure 7 presents the pseudo-code for a stencil program operating on dense D-dimensional arrays. It involves updating the “neighborhood” of each point of every array in a given region, denoted by \vec{l} and \vec{u} , with scaled values from other arrays. The neighborhood used to update array A_x from array A_y is defined by the stencil $S(x, y)$. At each time step t , every valid array index in each array x (i.e., bounded by \vec{l}_x and \vec{u}_x) can be updated from the array locations in the stencil neighborhood of all other arrays y using the coefficient function $c_{(x,y)}$. A distinct stencil coefficient function can be defined for each pair of arrays in an update operation. A temporary array TMP is employed to handle write-after-read dependencies in the array being updated. The DETECT_ERRORS() instantiates the required detectors for the corresponding time tile. In the case of program converging and exiting before finishing the entire loop of the time tile, there is an extra set of trailing detectors instantiated by DETECT_ERRORS at the loop exit for protection of the end segment of the computation.

```

1 //D-dimensional array type
2 using MultiDimArray = ...;
3 //stencil routine on N multi-dimensional arrays
4 auto stencil(MultiDimArray A[N]) {
5     for(int t=0; t += ρ) {
6         for(int tt=t; tt<t + ρ; tt++) { //in one time tile
7             if(converged) {
8                 DETECT_ERRORS(); //<--(Detector-2)
9                 return ;
10            }
11            for(int x=0; x<N; x++) { //every array
12                for(i | l̄ ≤ i ≤ h̄) //every valid index
13                    for(int y=0; y<N; y++) //every RHS array
14                        for(s̄ ∈ Sx,y) //the stencil
15                            TMP[i] += cx,y(s̄) * A[y][i + s̄]; //update
16                for(i | l̄ ≤ i ≤ h̄) //every valid index
17                    A[x][i] = TMP[i];
18            } //for 'x'
19        } // for 'tt'
20        DETECT_ERRORS(); //<--(Detector-1)
21    } // for 't'
22 }
    
```

Fig. 7. Stencil computation pseudo-code. A compiler can transform the code in lines 11–19 into any equivalent form. Detector-1 is used throughout the computation at the time tile boundaries. Detector-2 is used at the end of the computation.

Optimizations, and Overall Algorithm: As Figure 2 shows, we can determine a collection of inputs such as $[x - 4, t]$ that can be removed from consideration *because they have no effect within dp_T bits of precision*. This calculation is described in §4.

Our hope to leapfrog by T steps will not be realized unless we can “seal off” past computational points from future consideration. In §5, provide the analysis underlying this strategy. In our example stencil, it will allow us to shift the baseline by ρ steps as illustrated in Figure 3. The new baseline is obtained at ρ steps in the future while T is the leapfrogging step. In fact, the following is an invariant for any detector instantiation: $\forall(\rho, T) : \rho \leq T$.

Key highlights of our approach include: (1) rigorous floating-point precision analysis made possible by exploiting the structured nature of our computations, (2) being able to define concepts such as essential (E_w) and protected (P_w) widths that help us reduce the amount of computation necessary to achieve a certain level of protection, and (3) cost analysis for optimal detector deployment (explained in §5) for a given amount of protection.

3 APPLICATIONS

FPDETECT’s direct evaluation strategy has the ability to check bounds on the values generated in the stencil’s computational space at runtime. This can help trap software level bugs that may be introduced during compiler transformations. It also helps detect soft-errors within a thresholded precision limit providing robust and precise coverage of the compute space for protection against silent data corruption (SDC).

Parameter	Remark
$\vec{l} = \{l_1, \dots, l_D\}$	lower bound of array region
$\vec{u} = \{u_1, \dots, u_D\}$	upper bound of array region
N	number of arrays
ρ	time tile size
$S_{x,y} = \{\vec{s}_1, \dots, \vec{s}_n\}$	Stencil offsets to update each point of array A_x from points in A_y
$c_{x,y}(\vec{s})$	stencil coefficients to update array A_x using array A_y

Table 2. Stencil computation parameters. \vec{l}, \vec{u} , and \vec{s}_i contain integers. $N, T \in \mathbb{Z}^+$. Implicitly, $\forall \vec{s} \notin S_{x,y} : c_{x,y}(\vec{s}) = 0$. $\forall \vec{s}, x, y : c_{x,y}(\vec{s}) \in [-1, 1]$.

3.1 Software Bug Detection

Loop optimization frameworks generate optimized code for stencil programs. Pluto [7] performs polyhedral transformations that incorporate a host of optimizations to generate efficient code for stencils and other loop programs. Pochoir [47] is a compiler to generate efficient implementations of stencil computations from a high-level specification.

There has been a renewed interest, especially in the context of kernels such as stencils, in the generation of optimized programs that exploit various architectures (CPUs, GPUs, ..), instruction sets, and customized hardware such as FPGAs. The code generated by such tools needs to be checked to detect bugs in the toolchain early and avoid errors creeping into production code. While one ideally desires a fully verified toolchain, developing such toolchains is a non-trivial task. FPDETECT can be used as part of the testing toolchain for these tools as they are developed. Thus, FPDETECT can enable faulty compilers being identified and corrected before being used in production environments. Specifically, compiler transformed programs can harbor bugs, as shown in the work on Polychex [3]. Prior efforts have studied the design of approaches to verify or check the correctness of code generated by such optimizers [3, 39, 51]. These approaches detect bugs that impact the changes in control and data flow, with limited support for semantic transformations. Unlike the control or data flow based approaches, FPDETECT is not limited by the nature of the transformations employed and carefully captures the semantics of the stencil operations. On the downside, the analysis is imprecise in a different fashion than control or data flow analysis, which are not affected by the floating point round-off errors.

We show that, with respect to the benchmarks chosen, commonly considered loop transformation bugs can be trapped with around 2% overhead, allowing tested by unverified codes to be shipped to third-parties who may keep the detectors turned on till gaining sufficient trust.

3.2 Soft-Error Detection

FPDETECT is intrinsically designed and optimized to help protect applications by detecting SDCs with small enough detection latency. We consider a single event error model wherein a single error at some time t *transiently* corrupts one or more values of one or more participating arrays in the computation resulting in a soft-error. These errors are non-permanent (transient) in nature and cannot be replicated making them extremely difficult to detect and isolate.

The soft error detectors generated using the FPDETECT approach are, by construction, devoid of any modeling bias unlike those are generated through machine learning [44, 46] or time-series data analysis methods [17] which tend to reflect modeling bias. FPDETECT's detectors faithfully represent the evaluation of the stencil by sampling the actual data space sparsely. It computes the output generated by a stencil application by faithfully accounting for the precision contribution of each point in the detector's dependence cone (as noted in Section 2). FPDETECT enables the user with a parametric knob called the **user defined precision (udp)** using which they can define the required accuracy at the program output. Given a *udp* value of, say, 20, and a detector designed for T -step direct evaluation with an error bound of dp_T , FPDETECT finds the *minimal set of points which contribute at least 20 bits of precision to retain dp_T bits of precision at the detector*.

We actually develop two detection strategies in the context of FPDETECT. The first employs one direct evaluation and the other employs two direct evaluations. The latter is necessary given that the last leapfrogging step may not finish at a multiple of T steps; in those cases, the second direct evaluation provides the effect of a trailing detector at the end of the stencil computation.

Single-direct detector: At time t_0 , direct evaluation is used to compute the estimated value of a point $A_x[t_0 + T][\vec{i}]$, T time steps ahead. When the iterative stencil computation reaches time $t_0 + T$ and evaluates this point, it is compared with the previously estimated value. If the two values differ

more than can be ascribed to floating-point round-off error, it indicates an error impacting either the direct evaluation or in some part of the iterative evaluation leading to that point, triggering a soft-error detection event. This strategy involves a single additional dot-product. The error is detected after T time steps, requiring that the computation executes at least till time step $t_0 + T$.

Double-direct detector: Values at two time steps t_0 and $t_0 + t'$ can be used to estimate a value at a future time $t_0 + T$ ($T > t'$). This involves two direct evaluations, one each at time steps t_0 and $t_0 + t'$, whose estimates can be compared in the latter of the two time steps. This allows flexible detection and does not require that the iterative computation reach time $t_0 + T$. A mismatch between the two estimated values (beyond the bound on floating-point round-off error) indicates an error in the computation between time steps t_0 and $t_0 + t'$. This detection strategy requires two dot products, potentially doubling the overhead. We minimize the overall overhead by using the single-direct detector as much as possible, and use the double-direct detector only at the expected end of the computation (typically determined by monitoring convergence).

A *crucial efficiency consideration* built into FPDETECT is that it detects soft errors by placing detectors at time-tile boundaries (line 20 of Figure 7). This allows a programmer or an optimizer to transform the statements within each time tile into any semantically equivalent form. For example, a polyhedral optimizer (e.g., Pluto [7] or PolyOpt [50]) can optimize this stencil *without interference from the detector*.

4 OPTIMIZED DETECTOR SYNTHESIS

At a high level, FPDETECT operates by comparing the iterative and direct evaluations within dp_T bits of precision. However, during the time interval $t=t_0$ to $t=t_0 + T$, not all points in the detector's dependence cone contribute to dp_T bits of precision; this is because of the round-off effects of using (finite-precision) floating-point arithmetic. This allows us to selectively carve out points from the input space. Two key concepts⁶ introduced in this section—namely that of **Essential Width** (E_w) and **Protected Width** (P_w)—helps define the amount of computation that can be carved out while still offering our guarantees. Later in §5, we describe an optimized detector synthesis scheme based on these concepts.

FPDETECT works by synthesizing detectors for the expected ranges of binades that the computation begins with, and is also assumed to be present at every certified baseline. A T -step detector's support comprises of $(2 * T * \vec{w} + 1)$ points centered around \vec{x} , that is the points in $X_D = [\vec{x} - \vec{w}T, \vec{x} + \vec{w}T]$, where \vec{w} represents the footprint of one iteration of the stencil expressed as a vector to include higher dimensional spaces. Each point x_i in the X_D belongs to the tightest encompassing interval I . Upon multiplying each x_i by their respective T -step coefficients, c_i , generates separate intervals for each individual product term denoted as

$$[\underline{y}_i, \overline{y}_i] = [\min(c_i x_i, c_i \overline{x}_i), \max(c_i x_i, c_i \overline{x}_i)]$$

This results in a new set of N points, $Y = [y_1, y_2, \dots, y_N]$, where $N = (2T\vec{w} + 1)$.

Define summation $S_Y = \sum_{j=1}^N [y_j, \overline{y}_j]$ which falls in the interval $[S_Y, \overline{S}_Y]$. If $[y_i, \overline{y}_i]$ does not influence S_Y in the scope of dp_T , then point y_i is a candidate for removal. We do this pointwise analysis for each y_i . For this we define, $S_{Y \setminus i} = \sum_{j=1, \neq i}^N [y_j, \overline{y}_j]$ and its bounds as $[S_{Y \setminus i}, \overline{S}_{Y \setminus i}]$. Now define $d_{\min}(y_i)$ as the distance between the exponent of the lower bound of $S_{Y \setminus i}$ and the exponent of the upper bound for y_i :

$$d_{\min}(y_i) = \max(0, \exp(S_{Y \setminus i}) - \exp(\overline{y}_i)) \quad (3)$$

⁶These are presented in more detail as “**Precision Driven Optimizations**” in **Appendix B** of the supplementary material for the interested reader.

This equation and the next help check whether y_i 's *maximal* contribution manages to affect the *minimal contribution* from all the remaining points (if not, due to the exponent differences, the magnitude contributed by y_i gets “shifted out” during the process of normalizing the exponents while doing floating-point addition):

$$\text{maxContrib}_p(y_i, S_Y) = p - d_{\min}(y_i) \quad (4)$$

Equation (4) gives the maximal precision contribution of point y_i to the final sum S_Y when S_Y is computed up to p precision bits. A y_i becomes part of the exclusion set, if $\text{maxContrib}_p(y_i, S_Y) < 0$. Note that $y_i = (c_i \times x_i)$ already includes one multiplicative term adding an extra half ulp error to the analysis.

Now, for a detector placed at $A_u[\vec{x}, t_0 + T]$, we define **Essential Width** (E_w) as the width of the multidimensional rectangular region around \vec{x} such that the direct evaluation over E_w is *sufficient* to guarantee dp_T precision at the detector.⁷ Specifically, the region is defined by extents E_{wl} and E_{wr} such that $E_w = E_{wl} + E_{wr} + 1$. The caveat from equation (4) is that all such excluded candidates could *collectively* affect the output within the precision limits; therefore we must engage in an iterative process of considering subsets of points to carve out such that equation (5) holds. In the general case, E_w is a vector and is written \vec{E}_w . Figure 3 illustrates E_w for evaluation of a 1-D stencil over T-steps.

LEMMA 4.1. *In the absence of an error, direct evaluation over the essential width (E_w) ensures the correctness of the computation to at least dp_T bits of precision at the detector location.*

For all points in the region excluded from $E_w \forall \tilde{X} : \tilde{X} \subset ([\vec{x} \pm \vec{w}T] - \vec{E}_w)$, the following holds

$$\forall x_i \in \tilde{X} : \text{maxContrib}_{dp_T} \left(\sum (y_i = c_i \times x_i), S_Y \right) \leq 0 \quad (5)$$

One form of false positives involves detection of soft errors when no error affects any iteration point on which the detector depends (aka the detector's dependence cone). The preceding lemma guarantees that, despite the reduced evaluation cost, in the absence of errors affecting the dependence code, the direct evaluation is equivalent to the iterative evaluation within dp_T bits and no soft error notification (false alarms) is triggered.

Covering multiple points with a single detector: Protected Width (P_w): As depicted in Figure 5, each point inside the dependence cone of the detector has varying contribution depending on its effective path contribution. To guarantee that an error affecting a bit at an iteration point is detected by a detector protecting it, the minimum contribution of that bit must impact the dp bits at the detector. This will result in the values computed by iterative and direct evaluation being different, triggering a soft error notification.

To quantify the minimal possible influence a y_i has on the final sum S_Y , we define another distance metric $d_{\max}(y_i)$ as the distance between the exponent of the upper bound of $S_{Y \setminus i}$ and the lower bound of y_i .

$$d_{\max}(y_i) = \max(0, \exp(\overline{S_{Y \setminus i}}) - \exp(\underline{y_i})) \quad (6)$$

Then, the minimal influence y_i has on the final sum when computed correct to dp_T bits of precision is evaluated as

$$\text{minContrib}_{dp_T}(y_i, S_Y) = dp_T - d_{\max}(y_i) \quad (7)$$

A detector's reach can then be configured to guarantee an user defined precision (udp) by carving out a set Y_{udp} from X such that:

$$Y_{udp} = [y_i : \text{minContrib}_{dp_T}(y_i, S_Y) \geq udp, \quad y_i \in Y] \quad (8)$$

⁷The word “sufficient” is important because we might, in general, have non-contiguous chunks of inputs that can be discarded. In FPDETECT, we extend E_w to make it a contiguous region.

The most significant udp bits of precision of each point inside Y_{udp} is then protected if S_Y is evaluated correctly to dp_T bits of precision. Equation (8) leads to our primary soft-error detection model that provides the guarantee that an error affecting within the most significant udp bits of points inside Y_{udp} is detected. In our stencil model, for a detector placed at $A_u[\vec{x}, t_0 + T]$, we define **Protected Width** ($P_w(T, \rho, udp)$) as the width of a multidimensional rectangular region centered around \vec{x} such that with respect to a detector placed at time $t_0 + T$ and spatial position \vec{x} , for each $\vec{p} \in \vec{x} \pm P_w(T, \rho, udp)$ at time $t_0 + \rho$, the above guarantee holds.

LEMMA 4.2. *An error affecting any of the MSB udp bits of a point inside the protected width is detected.*

For a point y_i in y , if y_i belongs to Y_{udp} and its minimal precision contribution is p_i at the final output, then $p_i \geq udp$. If $y_i \in [y_i, \bar{y}_i]$, then an error, err_{y_i} affecting within the MSB udp bits will be bounded by $err_{y_i} \geq 2^{exp(\underline{y}_i) - p_i + 1}$. Since, we are matching dp_T bits at the detector, hence the threshold of detectable error is bounded by $2^{exp(\bar{S}_Y) - dp + 1}$.

For our guarantee to hold, generated error \geq error threshold. This means $2^{exp(\underline{y}_i) - p_i + 1} \geq 2^{exp(\bar{S}_Y) - dp + 1}$. Taking logarithms and simplifying the above terms leads to the following relation that must hold true for all points inside the P_w region: $exp(\bar{S}_Y) - exp(\underline{y}_i) \leq dp_T - p_i$, and $udp \leq p_i \leq dp_T - (exp(\bar{S}_Y) - exp(\underline{y}_i))$.

In determining the protected region, where a detector is used to protect iteration points in multiple time steps, we choose ρ such that the protected width chosen at ρ is also valid for all time points $t_0 \leq t \leq t_0 + \rho$:

$$\forall 0 \leq t \leq \rho : P_w(T, \rho, udp) \leq P_w(T, t, udp) \quad (9)$$

This enclosed region forms the protected region for the given detector location. Figure 3 illustrates the protected region in terms of P_w and ρ steps for a given udp .

Probabilistic detection: While the above strategy guarantees detection, the stencil structure and user-specified udp requirements can severely constrain the protection region, incurring high detection overheads. To further trade-off overheads for detection capability, we consider a detector that only provides the detection guarantee on only a fraction of the points in the protected region associated with a detector. Given a specified coverage requirement cov , we choose the protected width P_w such that the fraction of points with guaranteed protection is at least cov . An error impacting the MSB udp bits of an iteration point is guaranteed to be detected by its enclosing detector, if it is among the points for which the detection is guaranteed. Alternatively, such an error is detected with probability of at least cov .

5 OPTIMIZED DETECTOR PLACEMENT

Dampening errors: We consider a single event fault model wherein a single fault occurring at time t can transiently corrupt one or more participating arrays. Based on properties discussed in the preceding section, an error at time t escaping detection by the nearest set of detectors must have impacted less significant bits. Suppose the coefficient set $C = \{c_i\}_{i=1}^n$ denotes the set of forward contributions of a point in the stencil. Then Lemmas 5.1 and 5.2 given below hold under the following assumptions:

- $\forall i, |c_i| \leq 1$: This implies all forwards contributions move the error magnitude towards the least significant bits
- $\sum_i c_i \leq 1$: The collective error spread from an affected point to all neighboring points in the forward path is less than equal to itself

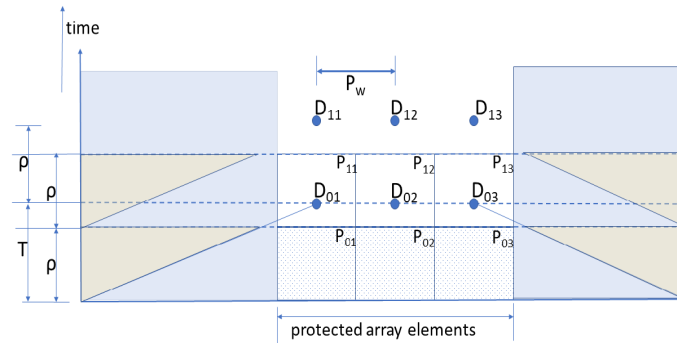


Fig. 8. Detector arrangement for a 1-d stencil. Horizontal: array elements; vertical: time steps

- There is no error cancellation within the scope of a detector. Multiple detectors may trigger a detection event as long as the triggering errors are localized to the scope of those detectors without any intervening error cancellations from its neighbors.⁸

The first two conditions are driven by the stability criteria and smoothening impact of the stencil.

LEMMA 5.1. *An error may never amplify in the forward path.*

LEMMA 5.2. *Error dampening guarantees an error missing detection does not affect future computations within the required precision limits.*

Under the dampening error model, the detectors can be arranged to cover the iteration space as follows:

- *Certified baselines:* Error dampening allows us treat all computations up to a time t that have passed the error detection checks as effectively being error-free. We will use these checked points at a given time step t as the new *certified baseline* to perform direct evaluation of the next detector.
- *Horizontal detector placement:* If a set of detectors is placed horizontally, i.e., at the same time step t , P_w apart in all dimensions, then the points at time t , once they pass the detection checks, will constitute a new certified baseline. Thus for a d -dimensional stencil of size $N = \{N_i\}_{i=1}^d$ along each dimension, if the detectors are placed $P_w = \{pw_i\}_{i=1}^d$ apart along each dimension, the number of detectors required is $\prod_{i=1}^d (N_i/pw_i)$.
- *Vertical detector placement: stacking.* Because the detector characteristics are influenced by the input range, at every baseline the input range needs to be computed. Alternatively, a bound on the input range can be predetermined based on the initial/boundary conditions and used for the entire computation. In both scenarios, the detectors can be vertically stacked to create new certified baselines as execution moves forward.

Illustration: Figure 8 illustrates the placement of detectors for the first two certified baselines for a 1-d stencil. D_{01} , D_{02} , etc. show the placement of the first set of detectors at time step T . These are computed from the array values at time step 0. D_{11} , \dots , the second set of detectors at time $T + \rho$, computed from the certified baseline at time step ρ . The detectors are vertically spaced ρ time steps apart, and horizontally spaced P_w apart. The protected regions are marked as squares and labeled at the right top. For example, P_{01} is the region protected by detector D_{01} . The shaded region denotes the boundary region unprotected by the detectors. Of this region, the shaded gray region has no influence on the detectors protecting points in that time step (outside their dependence cones). Errors in this region are not detected. The remaining region has an influence on at least one of the

⁸Such cancellations, if they occur, do not affect the final output.

detectors. Errors in these iteration points might be detected, but are not part of the guaranteed coverage.

$$\%cov = \prod_{i=1}^d \left(\frac{N_i - 2wT}{N_i} \right) * 100 \quad (10)$$

Boundaries: Although our method is applicable to the boundary points, the contributions from the boundary points need to be computed differently from the interior, incurring additional overhead. For cases where time dependent boundary conditions and Neumann boundary conditions [2] exist, FPDETECT lacks prior knowledge of how the boundary points are forced in the intermediate time tiles.

For fixed Dirichlet boundary conditions we can provide full coverage. To simplify the implementation, we ignore protection for the boundary regions in the generalized cases. Specifically, any computation point influenced by the boundary between certified baselines is not checked. Note that this reduces the maximum possible coverage to be below 100%, however still providing an accurate bound on the guaranteed coverage per equation (10) akin to probabilistic coverage that exemplifies the flexibility afforded by trade-off detection quality versus cost.

An error affecting such an unprotected region can spread to the rest of the computation space and result in erroneous output. This is akin to probabilistic coverage, with the probability of detection reduced by fraction of the total computation space left unprotected at the boundaries. Let N_i denote the problem size along i 'th-dimension in a d -dimensional problem. Equation (10) expresses the percentage of covered region for a detectors instantiated with $Tstep = T$. Here, w is the stencil width⁹.

Optimal detector configuration: For a given choice of detector, the essential width E_w is a function of the $Tstep$, the input exponent range, and the detector precision (dp). P_w additionally depends on udp and ρ . The cost function is evaluated as the relative cost with respect to the actual stencil evaluation. Section 6.1 details the cost function and the offline analysis used to construct optimal detector configurations.

6 OVERALL ALGORITHM

FPDETECT performs an offline maneuver to obtain a look-up table with optimal detectors configurations for the detectors. For each anticipated choice of udp , probability of detection, and anticipated input range, the offline analysis (§6.2) determines the detector configuration to be used during online execution. A detector configuration consists of: T , the distance at which the single-direct detector is evaluated; ρ , the number of iterations between certified baselines; E_w , the essential width to evaluate the detector; Detector coefficients for the support in the essential width; and P_w the spatial separation between detectors in the same time step. These parameters completely specify the detector configuration at runtime.

6.1 Offline Determination of Detector Configurations

Constraints on detector configuration: We use offline analysis to efficiently identify optimal detector configurations for use during online execution. To constrain the search space of possible configurations, we use an upper-bound on the $Tstep$ (say, $T_{max} = 256$ in our evaluation) that one might use for the detector evaluation. Larger $Tstep$ values are useful and often minimize the detector operational cost. However, this requires larger coefficient sets, needed for the direct evaluation, to be stored in memory. For a d -dimensional stencil with N -arrays, the space overhead encountered to store the effective coefficient space is $O(N \cdot T_{max}^{d+1})$. The range of udp values to be considered is bounded by the number of bits (1 – 53) and the maximum precision (dp) that can be preserved by both direct and iterative stencil evaluations informed by the round-off error analysis. We determine

⁹The implementation uses the exact expression, accounting for stencil asymmetry and non-Cartesian shapes.

the detector configurations for a finite set of coverage choices between 0% and 100%, corresponding to the fraction of points in a detector's protected region that are protected to the desired *udp* bits. The actual coverage including the boundary is computed online.

Relativized input exponent ranges: Consider two exact floating point numbers represented in triplet form as $a_f = (s_a, m_a, e_a)$ and $b_f = (s_b, m_b, e_b)$ where the mantissa m_a and m_b are represented in $p = 53$ bits. For a floating point addition (subtraction), the mantissa of the number with the lower of the two exponents has to be shifted by $|e_a - e_b|$ to match their exponent values. Thus, the binary addition (subtraction) of the mantissa depends the relative distance between the exponents for shifting (not on actual exponents).

In stencils, update rules are modeled as weighted sums involving only addition (subtraction based on sign) and multiplication. Multiplication by exact scalars involves binary multiplication of the mantissa, followed by addition of the exponent terms, maintaining linearity in the exponents. For example, let the coefficients associated with a_f and b_f be $\alpha_1 = (s_{\alpha_1}, m_{\alpha_1}, e_{\alpha_1})$ and $\alpha_2 = (s_{\alpha_2}, m_{\alpha_2}, e_{\alpha_2})$, respectively. The product $\alpha_1 a_f$ will have an exponent of $(e_{\alpha_1} + e_a)$ and $\alpha_2 b_f$ will have $(e_{\alpha_2} + e_b)$. Thus, the relative distance of exponents between these two terms will $|(e_{\alpha_1} - e_{\alpha_2}) + (e_a - e_b)|$ which depends essentially on the coefficient's exponents (that remain unchanged) and the relative operand exponent differences.

This fact can be utilized to map different interval ranges to some canonical exponent range that models the maximum relative distance of points inside the interval. To do this, we scan the input to find the smallest data point (in magnitude) and the largest data point (in magnitude) and characterize that interval with the exponent difference between these two data points. For an input interval, if (m_a, e_a) represents the smallest value (in magnitude) and (m_b, e_b) is the largest value (in magnitude) seen in the interval, then factoring out e_a produces the following mapping

$$[(m_a, e_a), (m_b, e_b)] \equiv (1, e_a)[(m_a, 0), (m_b, e_b - e_a)]$$

We can further factor out the corresponding mantissa and increment the mapped exponent interval width by 1 to have a larger bounding interval for the given input range. Since our analysis is conservative, bounds that hold for larger exponent ranges also hold for smaller exponent ranges.

$$[(m_a, e_a), (m_b, e_b)] \equiv (m_a, e_a)[(1, 0), (\frac{m_b}{m_a}, e_b - e_a)] \equiv [(1, 0), (1, e_b - e_a + 1)] \quad (11)$$

The operation of a stencil on an input range can be *relativized* to a small number of canonical exponent ranges. This allows us to use the offline analysis performed on specific exponent ranges on different set of actual exponents that belong to the same range. In our experimental setup, we profiled exponent ranges from 0 through 20 ($exp_{max} = 20$). The maximum *udp* is set as 40. Given the range of exponents and *udp* choices, the offline algorithm construct a lookup table that returns a 5-tuple (T, ρ, dp, P_w, E_w) corresponding to an optimal detector configuration for the given interval, required *udp*, and minimum detection probability.

Offline algorithm:¹⁰ We consider all T and ρ such that $T \leq T_{max}, \rho < T$. For a d -dimensional stencil, P_w is d -dimensional vector, corresponding to protected region of iteration points centered at the detector. E_w is represented by a rectangular region with a computed number of points along left and right of the detector along each direction. The cost function is derived as the ratio of the total detector overhead to the total cost of the stencil application evaluation. Post simplification of the cost function for a 5-tuple detector configuration ($exp, udp, T, \rho, Coeffs$) is given as

¹⁰The algorithmic listing is available in the supplementary material (Appendix C).

$$Cost = \frac{1}{\rho} \prod_{i=1}^d \left(\frac{ew_i}{pw_i} \right) \quad (12)$$

derived fraction of overhead cost to total stencil compute cost. Even though the tuple elements exp , T , udp , and $Coef fs$ do not explicitly appear in the cost function, they implicitly influence the cost through E_w and P_w . The algorithm takes as input parameters for which an offline profiles need to be determined: the maximum number of time steps ($Tmax$), the set of input ranges (as exponents in exp_set), set of udp values (as udp_set), and probabilistic coverage values (cov_set). The algorithm determines the configurations one input range choice at a time. Using floating-point round-off analysis, the maximum number of bits that will be preserved for each possible time step t is computed (as $maxdp$). For each t , the cost of evaluating each detector is computed as the product of the E_w dimensions to guarantee $maxdp[t]$ bits of precision of the direct evaluation t time steps away. Then, for each candidate protected region, the fraction of points with guaranteed coverage of b bits (where b is a candidate udp in the input parameter udp_set) is computed. If this fraction is greater than a desired coverage and if the associated cost is lower than that of any configuration seen thus far, this configuration is chosen. After evaluating all feasible solutions, the algorithm returns the last chosen configurations.

The cost of the offline procedure is dominated by dimensionality of the space to be explored. While this exhaustive evaluation of every feasible configuration can be expensive, for the benchmarks considered (in the next section), each offline procedure completes within several minutes. Search-space exploration techniques might further lower this cost.

6.2 Online Detector-Embedded Execution

We briefly discuss the algorithm¹⁰ to obtain the detector configurations and embed the detectors within the original stencil code. During online deployment of FPDETECT’s detectors, the input values are scanned to compute the input exponent range to be handled in the floating-point space. To account for the unprotected boundary regions, FPDETECT maps user’s input coverage value to an *equivalent internal coverage value* (as in_cov) that corresponds to the detection probability on the grid excluding the boundaries. The adjustment is done with the guarantee that the *fraction of points covered due to (in_cov) is at least as many required by cov over the entire computation space*. If FPDETECT fails to find an equivalent mapping, it conveys an error message for unsupported coverage. The input range, user-specified udp , and modified detection probability (in_cov) are used to lookup the detector configuration.

After an initial evaluation of the detector and the stencil for ρ iterations, the execution of the stencil is split into two segments: iterations till the next detector evaluation ($eval_detector$) and iterations till the next detector check ($detector_check$). Thus, the stencil is executed with *interleaved detector evaluation and checking*. Note that the algorithm assumes ρ is greater than half the detector evaluation T-step. This scenario requires at most two “live”, i.e., unchecked detectors per spatial position in the iteration space, at any time. If not, at each spatial position, multiple detectors need to be evaluated and retained until they are checked. When all iterations have been executed, the iterations past the last certified baseline need to be checked. These leftover iterations are checked using the trailing detection strategy.

7 EVALUATION

Benchmarks: We evaluate FPDETECT on the stencil kernels shown in Figure 9. We choose a set of benchmark problems from elliptic, parabolic, and hyperbolic PDEs evaluated as stencils using the explicit finite difference method. Benchmark examples considered are Poisson equation with different combinations of Dirichlet and Neumann boundary conditions, heat equation with different initial and boundary conditions, and second-order wave and convection-diffusion equations. Our error analysis and optimization techniques are based on the input data interval and not the exact

Parabolic (heat): $\frac{\partial u}{\partial t} = \nabla^2 u(x, y) + f$ $\alpha = 3, \zeta = 1.2$	[Dirichlet initial/boundary condition] h1. $f = \zeta - 2 - 2\alpha, u = 1 + x^2 + \alpha y^2 + \zeta t$ h2. $f = 0, u = 1 + x^2 + \alpha y^2 + \zeta t$ h3. $f = 2\zeta - 2 - 2\alpha,$ $u = 1 + x^2 + \alpha y^2 + \zeta t^2$	[Neumann initial/boundary condition] $f = 0$ h4. $u(x, y, t) = e^{-\pi^2 t/2} \sin \pi(\frac{x+y}{2})$ h5. $u(x, y, t) = 4 + e^{-\pi^2 t/2} \cos \pi(\frac{x+y}{2})$ h6. $u(x, y, t) = 2 + e^{-\pi^2 t/2} [\sin \pi(\frac{x+y}{2}) + \cos \pi(\frac{x+y}{2})]$
Poisson equation: $-\frac{\partial^2 u}{\partial x^2} - \frac{\partial^2 u}{\partial y^2} = \text{RHS}$	[Deflection in a membrane] $p_1 = 4e^{-5((x-0.6)^2+(y-0.6)^2)}$ $p_2 = 2e^{-5((x-0.3)^2+(y-0.3)^2)}$ $p_3 = 4e^{-5((x-0.3)^2+(y-0.6)^2)}$ p4. $\text{RHS} = p_1, u = 0$ p5. $\text{RHS} = p_1 + p_2, u = 0$ p6. $\text{RHS} = p_1 + p_2 + p_3, u = 0$	[Neumann initial/boundary condition] p7. $\text{RHS} = 10e^{-\frac{(x-0.5)^2+(y-0.5)^2}{0.02}}, \frac{\partial u}{\partial n}(x, y) = -\sin(5x)$ p8. $\text{RHS} = 0, \frac{\partial u}{\partial n}(x, y) = -\sin(5x)$ p9. $\text{RHS} = 20e^{-\frac{(x-0.25)^2+(y-0.25)^2}{0.01}}, \frac{\partial u}{\partial n}(x, y) = -\sin(5x)$
[Dirichlet initial/boundary condition] p1. $\text{RHS} = -6, u = 1 + x^2 + y^2$ p2. $\text{RHS} = -6(2+x+y), u = 1 + x^3 + y^3$ p3. $\text{RHS} = -2 - 12y, u = 1 + x^2 + 2y^3$	[initial and boundary conditions: $c = 0.7,$ $\frac{\partial u}{\partial t} = 0]$	Hyperbolic (convection diffusion): $\frac{\partial u}{\partial t} + \alpha \nabla u(x, y) = \zeta \nabla^2 u(x, y)$ initial/boundary condition from $u(x, y, t) = \frac{1}{4t+1} e^{-\frac{(x-\alpha t-0.5)^2-(y-\alpha t-0.5)^2}{\zeta(4t+1)}}$ c1. $\alpha = 0.8, \zeta = 0.01$ c2. $\alpha = 0.4, \zeta = 0.4$ c3. $\alpha = 0.1, \zeta = 0.8$

Fig. 9. Benchmark PDEs (p1–p9, h1–h6, w1–w3, c1–c3) solved using the stencil finite-difference method. Initial and boundary conditions are derived from the equations provided. All stencils span the $[0, 1]$ spatial domain and are run 4000 time steps.

values. We test our hypothesis rigorously by exercising each benchmark equation with multiple initial and boundary conditions. In addition to the exponent and sign bits, fault-injection-based evaluation was conducted for a user-defined precision of 15 mantissa bits. This corresponds to a total protection of 27 most significant bits.

Experimental setup: All benchmarks are compiled using ICC 18.0.5 with `-qopenmp -O3` options and executed on dual 14-core Intel Xeon CPU E5-2680v4 2.60GHz CPUs system (total 28 processor cores) with 64GB of RAM. The Pluto optimized code were generated with ‘PLUTO version 0.11.4-350-g8debc44’.

Detector coverage excluding boundaries: To reduce the complexity of the detection strategy, we did not protect statement instances impacted by the boundary between certified baselines. This limits the maximum coverage that can be guaranteed by our implementation. For all benchmarks and configurations evaluated, we observed this fraction to be greater than 90% of the computation space, demonstrating the simplification does not significantly limit detection ability.

Space overheads: At stencil runtime, FPDETECT requires space to store:

- the set of all possible coefficients of interest,
- the direct evaluation configurations for specific input ranges and precision needs, and
- the result of the selective direct evaluation by each detector.

We bound the offline analysis with $T_{\max}=256$ iterations and require the full coefficient set for $T=0$ to T_{\max} . This allows a runtime choice of time tile size between 1 and 256. This incurs a space overhead of 128MB. While incurring a large memory footprint, only a fraction of this data—one

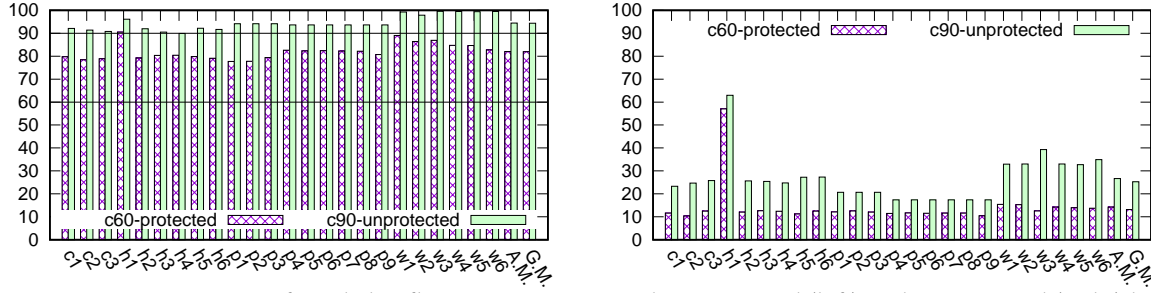


Fig. 10. Detection rates of single bit-flip error injections in bits protected (left) and unprotected (right) by the detector (A.M.: arithmetic mean; G.M.: geometric mean)

rectangular portion the single-direct detector—is used during online execution and the accessed portions are reused for all detectors at a time step. In addition, the trailing detector accesses one rectangular portion determined by the number of iterations not executed by the last tile. This results in good cache behavior, limiting their impact on overall performance.

The offline configuration lookup table is built by profiling over 20 exponents, 40 *udp* and coverage values from 0 to 100% (in increments of 5%). Thus, the offline lookup table is indexed by a 3-tuple of (exp, udp, cov) , with each lookup returning a 6-tuple configuration of $(T, \rho, dp, \vec{P}_w, \vec{E}_{wl}, \vec{E}_{wr})$, where \vec{E}_{wl} , \vec{E}_{wr} , and \vec{P}_w are d -dimensional vectors for a d -dimensional stencil program. Here, \vec{E}_{wl} and \vec{E}_{wr} corresponds to the left and right extents of E_w .¹¹ FPDETECT scans the data at runtime to determine the necessary exponent range. This is combined with the user-specified precision and coverage to index the lookup table and obtain the corresponding detector configuration. For a 2-dimensional problem, a key-value pair in the table occupies a space of 48 bytes. Over all the profiled configurations, the configuration lookup table requires a total space of ≈ 750 KB per benchmark.

In addition to the coefficients and the lookup table, we require one floating-point number per array at each detector location to store the value computed through selective direct evaluation. The maximum number of instantiated detectors comes to around 387K for the wave benchmarks. For most other benchmarks is around 100K for a problem size of $10K \times 10K$ and $T_{max} = 256$.

7.1 Software Bug Detection

We evaluate the effectiveness of FPDETECT in detecting logical errors injected into the code generated for the stencil programs in Table 9 optimized by Pluto [8]. Specifically, we inject three classes of bugs injected in the evaluation of PolyCheck [3], a tool designed to check errors introduced by loop transformers: incorrect loop bounds, invalid array accesses, and invalid loop reorderings.

For each software bug introduced, we evaluated its impact using bitwise comparison of the result with that of the non-buggy version. Any mismatch is treated as a bug. Some bugs might not result in an erroneous result for the problem instances evaluated. FPDETECT cannot aid in their detection.

The bugs introduced in the source potentially affect multiple runtime operations, making them easier to detect than soft errors. Exploiting this, we evaluate FPDETECT’s effectiveness in detecting software bugs when deployed with a small *udp* value of 4. For each benchmark, the default detector precision (*dp*) determined for this *udp* is used in the evaluation.

Pluto-generated code: To generate optimized versions using Pluto, we implemented all the stencils in the form of affine loop nests enclosed in *scop* pragmas. This code input to Pluto has consists of median 53 source lines of code (SLOC)¹² per benchmark. Pluto takes these *scop*-annotated benchmarks as input to generate optimized versions with median 1157 SLOC. The median of the number of loops in the transformed code was 365 across all the benchmarks with a median

¹¹ \vec{E}_{wl} and \vec{E}_{wr} are equal in the case of symmetric stencils.

¹² Source lines of code are measured using *sloccount* tool

nesting depth of 6. In checking such large and complex generated codes, tools such as FPDETECT are essential.

Loop bound and array access bugs: We automated the injection of loop bound bugs. For loop bounds, the injected bug either offsets the lower bound by one in the positive direction or offsets the upper bound by one in the negative direction. We automated the injection of array access bugs. Specifically, array accesses were made incorrect by either dividing or multiplying the indexing term by two.

False positives: Some bugs do not result in any difference in our bitwise comparison of the result with the non-buggy version. Therefore, our approach incurs no false positives in our evaluation. This is because some source-level bugs do not manifest at runtime. For example, a loop iterator might be constrained by multiple loop bounds (e.g., min or max of multiple expressions), with the loop bound never reaching the error-injected expressions.¹³ In a situation with multiply nested loops where the indexing for an inner loop depends conditionally on outerloop indices, a bug impacting the outer loop bound doesn't often affect the inner loop and hence doesn't impact the stencil's output.

Table 3 summarizes FPDETECT's bug detection effectiveness for the above two categories of bugs. The table only lists detection percentages when the bitwise comparison with the non-buggy version flags an error-injected version as being in error.

Table 3. Software bug detection results.

	Loop bound			Array access			Loop bound			Array access			
	#SL	#RL	%det	#SL	#RL	%det	#SL	#RL	%det	#SL	#RL	%det	
H1	374	374	100	300	267	99	H2	370	370	100	300	258	100
H3	374	374	100	300	267	98	H4	486	106	99	300	26	100
H5	486	106	100	300	26	100	H6	486	106	100	300	26	100
P1	10	10	100	18	17	100	P2	12	12	100	18	17	100
P3	12	12	100	18	17	100	P4	370	310	100	300	223	87
P5	370	310	96	300	223	82	P6	370	310	96	300	223	82
P7	414	104	98	300	48	97	P8	416	104	100	300	44	98
P9	416	104	98	300	44	98	W1	360	280	100	300	215	55
W2	360	280	44	11	6	54	W3	360	350	31	300	266	45
W4	260	280	45	300	215	60	W5	360	280	53	300	215	62
W6	360	350	100	300	266	100	C1	360	360	100	300	262	100
C2	360	360	100	300	262	100	C3	360	360	100	300	262	100

The #SL enumerate all the possible source locations for the types of bug injected. #RL enumerates the number of source locations that were reached at runtime. %det denotes the fraction of errors flagged by bitwise comparison with correct execution that was detected by FPDETECT. We observe that FPDETECT has a high but not perfect detection rate. We investigated the scenarios in which FPDETECT missed detection and all of them were a result of the logical error having a low impact on the stencil's output. Specifically, the impacted point's effect on the stencil was beyond the required detector precision (dp) evaluated by our conservative error analysis.

To illustrate, consider two cases where FPDETECT detect such an impact and another where it escapes FPDETECT's detection. In the first case, the detector evaluates to the expected value to $0x40101b539cbac780$ (we present in hex values for readability), while the bug affected stencil

¹³An example can be found in the supplementary material in Appendix D.

computes `0x40101b53a11cf49f`. They match in the first 23 bits of the mantissa. This example, evaluated for $W1$ has $dp = 30$, hence is trapped. In the second scenario, detector evaluate the expected value to `0x4004178de3e4ab00` while the buggy stencil evaluates `0x4004178de3e4aac4`, differing in only the last 9 bits of mantissa. Given the low detector precision of 30 for wave benchmarks, this error goes undetected. In general, our conservative error analysis and low udp choice predicts only upto dp bits at the detector, attributing precision beyond dp bits to round-off errors. While this leads to missed detection opportunities, we still observe high detection rates.

Loop order bugs: Unlike changes to array accesses and loop bounds, changing loop orders required non-local changes to the Pluto-generated code. Therefore, we handcrafted the error injected versions. The handcrafted scenarios included swapping nested loop pairs and re-ordering of non-nested loop blocks. The optimized codes included a maximum of 360 nested for loops with a maximum loop nesting depth of 11. Testing all possible combinations of loop reorderings will be prohibitively expensive. We limited our testing to 15 loop order bug injections per benchmark.

Across all benchmarks, a median of 3 injected bugs per benchmark did not result in a bitwise difference in the output. This could either be due to the reordered version being correct due to commutativity of loops, or the error being too small to persist under finite precision arithmetic for the inputs chosen. These bugs were also not detected by FPDETECT. Other than benchmarks $W1$ and $W3$, loop order bugs injected in all other benchmarks were detected. In $W1$ and $W3$, there was one injected bug in each that resulted in the bitwise comparison flagging an error was not detected by FPDETECT. In both cases, the difference was within 8 least significant bits (corresponding to $< 10^{-12}$ relative error), and could not distinguished from floating point round-off errors.

In summary, we observe that FPDETECT can detect a large class of software bugs with a low udp of as low as 4 bits. In all cases evaluated, we observed negligible overheads ($< 2\%$), making it a useful component in a test suite or as a low cost online checking tool for flagging systematic errors. As observed earlier, increasing the udp and dp can improve the percentage of bugs detected, at the cost of greater runtime overheads. Note the a change of udp only changes the number of points being sampled for detection. The P_w corresponding to this udp only decides the relative distance between the sampled points.

Soft error detection: We performed fault injection experiments to validate the coverage guarantees provided by FPDETECT. Single bit flips were injected in the kernel source code by corrupting array locations involved in the stencil computation. Such a fault model abstracts the cause of the fault to an anomalous behaviour in data evolution. FPDETECT is designed to detect an anomalous behaviour in data evolution with a precision guarantee irrespective of where it originates as long as it impacts the computation. The time steps and bit locations subject to injection were selected randomly with equal probability across the iteration space, array index space, and bit locations. The bit flips were injected with equal probability on all array locations, including the unprotected boundaries. Each benchmark was exercised through a fault injection campaign comprising of 10,000 executions to determine the detection rate. In the reported results, FPDETECT was evaluated for detector configurations guaranteeing 15 bits of mantissa precision (total of most significant 27 bits including 11 exponent bits and 1 sign bit) with a coverage of 60–90%.

We observe that, across all benchmarks and including the boundary region, errors injected within the most significant udp bits (the guaranteed protection) were detected 92–99% of the cases for the 90% coverage, and 78–90% of the cases for the 60% coverage configuration. We observed similar trends when multiple errors are injected, at multiple and randomly selected locations in the iteration space. Figure 10 shows the detection rates for the two coverage scenarios when only considering error affecting the protected region (the most significant 15 bits, labeled “protected”) and only those affecting the unprotected region (labeled “unprotected”). Furthermore, we observe

that flips in bits beyond the unprotected region (not guaranteed to be detected) were detected on average 26% (13%) of the cases for 90% (60%) coverage scenario. Hence, even with a conservative configuration for guaranteeing user-defined bits of protection, in practice, our approach *empirically* protects a larger fraction of the computation space and error scenarios.

Recent studies [?] show that single-bit errors yield a higher percentage of SDCs in most cases, compared to multi-bit errors. In cases of data corruption, two or more bit flips in the opposite direction, can reduce the overall error magnitude thus filtering it out of the detectable range. We performed a small scale multi bit-flip experiment to check FPDETECT's detection ability in such scenarios over a selected number of representative benchmarks for a coverage guarantee of 90%. Furthermore, the space of multi bit-flip errors is seemingly large. We restrict ourselves to double bit-flip errors. Each injection campaign executed at a random time step, splits the data array into 16 byte sections and selects one section randomly within which 2 randoms bits are flipped.

For multi bit-flip campaigns including atleast one bit flipped inside the protected range, errors were detected in 88-99% of the cases. Furthermore, multi bit-flips encountered outside the protection range were detected on average for 36% of the cases. Hence, even though our guarantees are restricted to single bit errors, empirically the detectors can handle multi bit errors.

Comparative study: Our detector synthesis strategy provides a variety of tuning knobs for flexibility in terms of minimum precision and protection coverage with precise bounds. To ascertain the effectiveness of our tool, we compare them with two state-of-the-art soft error detectors, AID [17] and SSD [45], which build data value centric model for soft error detection.

SSD builds an epsilon-insensitive support vector machine regression model to detect SDCs. As spatial features, it includes values of a given point's neighboring data points as the training data. It runs into scalability issues by requiring the generation of data traces of every point in the simulation over all time steps before being fed to the learning model. We had to scale down the problem to a small size of $1k$ points per dimension. It learns the classifier first, triggering false positives for early stages of the simulation trace. In particular, we encountered false positives in initial one to five iterations. Hence, we devised the fault injection mechanism after atleast 10 iterations have passed. SSD did not trigger a detection in any of our error-injected runs past the first 10 iterations. We believe, in these benchmarks, the variations observed in the first few iterations make SSD consider the error-injected behavior appear normal.

AID is an adaptive SDC detector wherein a best-fit prediction model gets selected adaptively based on local online data. AID faired better with our benchmarks than SSD. However, the detection rates and overheads were extremely conservative. The comparative analysis by Kestor et al. [31] reports significant slowdown at a maximum of $1.4\times$ for AID when snapshots were taken for every time step. We observed similar overheads when taking snapshots at every step. To reduce the overhead, we performed two experiments with snapshot every 3 steps and every 10 steps. In the former case, AID reported similar overheads averaging around 80% with a maximum detection rate of 54%. In the latter case, the overhead reduced to the 20 – 30% range, while the average detection rate was around 25% with a maximum and minimum of 37% and 21%, respectively.

Sequential overheads: Figure 11 shows the sequential execution overheads of our detection approach for three *udp*-coverage configurations: 10, 15, and 20 bits. We observe that the overhead depends on the user-required coverage guarantee, with overheads, in general, below 10% for *udp*=15 and 80% coverage, for heat, Poisson, and convection-diffusion benchmarks. Overall, we observe that protecting additional bits or providing greater coverage increases the overhead. All wave benchmarks (and some Poisson benchmarks for 90% coverage) incur far greater overheads, reaching over 60% for *udp* of 20 bits and 90% coverage. This is due to the nature of the stencils that, as discuss below, leads to a sharp reduction in the protected region (Figure 12). Despite this increase,

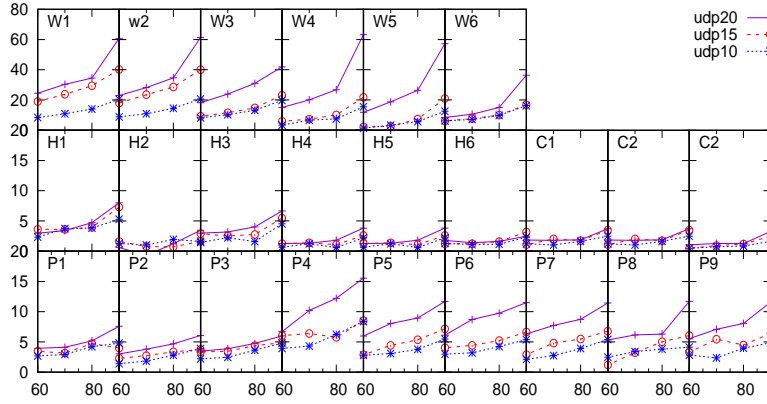


Fig. 11. Sequential benchmark execution overheads for three different user-defined precision (*udp*) values (20, 15, and 10) and varying coverage; y-axis: execution time overhead in percentages.

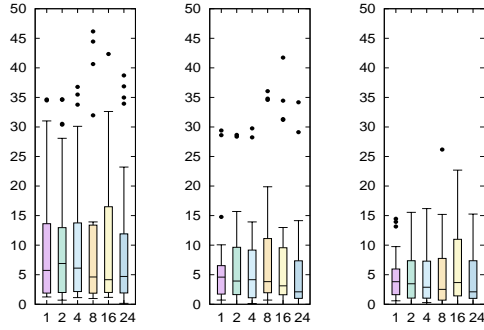


Fig. 13. Detection overheads across all benchmarks for 80% coverage for *udp* values 20, 15 and 10. x-axis: thread count; y-axis: execution overhead in percentage.

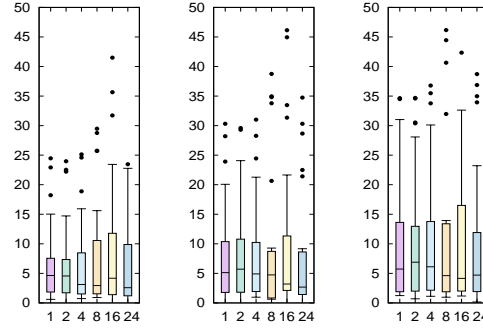


Fig. 14. Detection overheads across all benchmarks for *udp* 20 and coverage of 60%, 70% and 80%. x-axis: thread count; y-axis: execution time overheads in percentage.

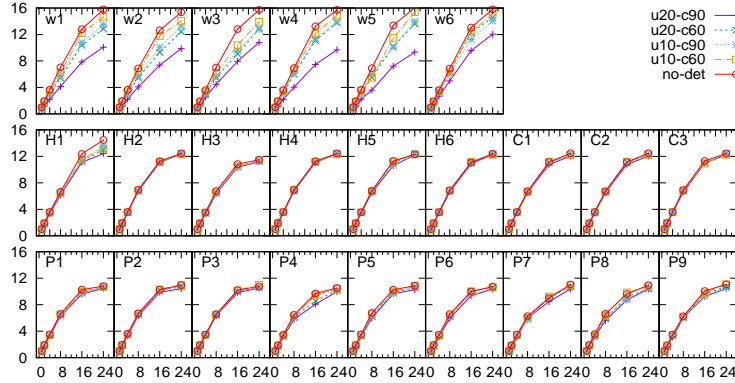


Fig. 15. Scaling on up to 24 threads for the baseline without detectors and with detectors over three combinations of *udp* and coverage [(*u=udp,c=cov*)=(20,90), (10,90), (20,60), (10,60)]. x-axis: thread count; y-axis: speedup over single-threaded execution with no detectors.

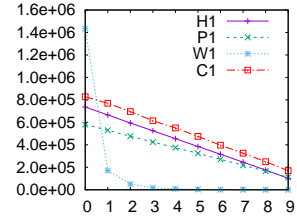


Fig. 12. Protected region volume per detector (optimal configuration) with input exponent range for four benchmarks, *udp*=15 and 80% coverage. x-axis: exponent range ($2^0, 2^1, \dots$); y-axis: number of iteration points in the protected region per detector.

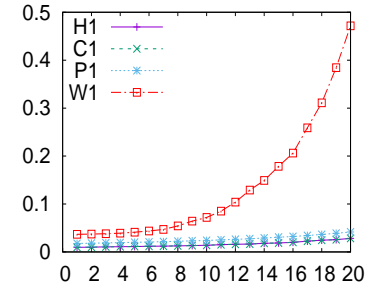


Fig. 16. Optimal cost from Equation (12) (y-axis) vs *udp* (x-axis) for four benchmarks.

these results demonstrate the approach’s flexibility in supporting low detection guarantees when a reduced overhead is desired.

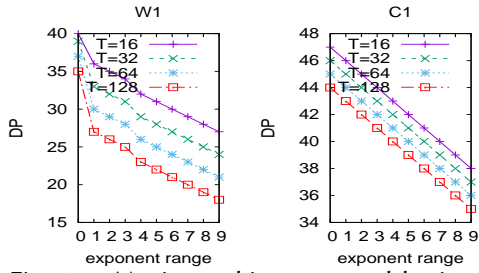


Fig. 17. Maximum bits preserved by iterative stencil (y-axis) as function of input exponent range (x-axis), determined by our analysis, for two benchmarks (w1 and c1) for different maximum T-step choices.

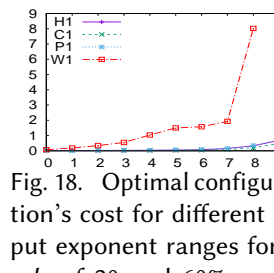


Fig. 18. Optimal configuration's cost for different input exponent ranges for a udp of 20 and 60% coverage. x-axis: input exponent range ($2^0, 2^1, \dots$); y-axis: cost for optimal configuration (from Equation (12)).

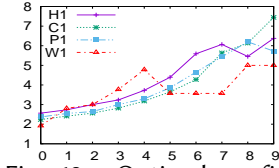


Fig. 19. Optimal configuration's E_w to P_w ratio for different input exponent ranges for a udp of 20 and 90% coverage. x-axis: input exponent range ($2^0, 2^1, \dots$); y-axis: E_w/P_w for optimal configuration (from Equation (12)).

Scalability: Figure 15 shows the scalability of the baseline and detector-embedded versions on up to 24 threads using OpenMP. Across all benchmarks, both variants achieve similar speedups, demonstrating that the detectors do not interfere with efficient parallel execution. While not shown here, we observed similar trends (in terms of low overheads) with various thread counts for other user-defined precision and coverage values.

For the wave (“W”) benchmarks which model hyperbolic PDE equations we encounter reduced scalability for stricter configurations of high udp and coverage. We believe this is due to higher udp values requiring more detectors. This coupled with the larger E_w results in potentially increased cache contention and hence the associated reduced scalability.

Summarizing the overheads, Figure 13 shows the distribution of overheads for 80% coverage and three udp values. Figure 14 shows the distribution of overheads for a fixed udp (20) and three different coverage percentages. In both cases, we observe greater coverage percentage or udp requirement can increase overheads. However, the median overhead remains close to 5% and does not increase with scale.

Table 4 summarizes the optimal configuration, detection rates and overhead factors for user defined protection goals requiring $udp = 20$ and 90% coverage. We select the summary for a subset of the example benchmarks that have shown the largest variations in their configuration and detection rates in their class of numerical kernels.

Benchmark	optimal config		% det		% Seq ovh	Scalability factor		
	(T, dp_T)	(ew, pw)	single bit	Multi bit		k=2	k=8	k=24
H1	(254,39)	(63,14)	96.14	94.66	8.0	1.76	6.18	12.41
H4	(256,38)	(63,14)	90.47	88.54	3.81	1.84	6.54	12.03
P1	(160,40)	(69,24)	94.12	93.88	7.59	1.78	6.27	10.41
P4	(160,37)	(69,17)	93.65	94.92	15.55	1.67	5.78	9.96
P7	(160,37)	(69,17)	93.65	95.05	11.43	1.65	6.02	10.35
W1	(10,36)	(20,3)	99.25	99.48	60.78	1.20	4.13	10.07
W4	(10,36)	(20,6)	99.25	99.74	41.91	1.15	4.03	9.67
C1	(250,38)	(66,15)	92.10	90.76	3.72	1.82	6.54	12.03

Table 4. Summary table for optimal configurations, detection rate, sequential overhead overhead and scalability factors for udp of 20 and coverage 90%

7.2 Analysis of the Overhead Cost Function

Because FPDETECT’s detection strategy is sensitive to the specific stencil and the characteristics of the initial/boundary conditions, we have chosen multiple benchmarks and configurations, including different initial and mixed boundary conditions. For a broader analysis of the space of choices evaluated in the offline phase, we examine four candidate benchmarks—h1, c1, w1, and p1—in detail.

Variation of essential and protected widths: Figure 12 shows the variation in optimal P_w volume with input exponent range. W1, a second-order wave equation representing hyperbolic PDEs, exhibits the highest overhead and cost since its P_w volume rapidly diminishes with increasing exponent sizes. Benchmarks h1 and c1 exhibit a slower change in the optimal P_w .

Figure 19 plots the ratio of E_w to P_w for their optimal configuration with varying input exponent range for a fixed udp and cov . Larger binade differences in the input values result in increasing separation between the E_w and P_w values, often increasing the E_w to P_w ratio. Together with ρ (equation (12)) this can potentially lead to an increase in detector overhead.

Impact of input range and udp : Figure 18 shows the cost function values for four benchmarks (h1, c1, p1 and w1) for hypothetical range of input values from 2^0 to 2^9 and user-defined precision of 20 bits. We observe that cost increases with input range, especially for w1. Thus, accurate yet efficient evaluation of the input range can help reduce the detector overheads.

Figure 16 shows the evaluated cost function value as udp is varied. Similar to the input exponent range, we observe that some benchmarks (especially w1) are more sensitive than others to increase in udp . Thus, careful choice of udp can maximize coverage while minimizing overhead.

8 ADDITIONAL RELATED WORK

Floating-point error analysis was the central driving concept in our work. Boldo [5, 6], Darulova [14], Magron [34], and Solovyev [43] are three recent pieces of work that conduct rigorous error analysis. Zhang [55] uses *reduced precision check* to detect errors in the floating point units as a hardware solution. Daumas et al. reason about floating-point operations using interval arithmetic [15]. These tools focus on programs operating on fixed and small number of inputs. They are unable to handle the kinds of complexity presented by stencil expressions unfolded in time. They also do not steer their analysis toward the synthesis of online error detectors like in this work.

We exploit the structure of stencil operations to simplify analysis of *parametrically* sized programs. Kramer established worst-case bounds for interval arithmetic [32]. We build on the guarantees for individual operations (IEEE 754 [30]) to analyze worst-case bounds for stencil programs.

Chisel [35] and Rely [10] consider potentially erroneous execution of portions of a program by analyzing the probability of the output being erroneous. They track the probability of an erroneous output rather than its magnitude. Soft error analysis has been performed for specific algorithm classes (e.g., linear algebra [52, 53] and iterative solvers [20, 48]). Huang and Abraham introduced algorithm-based fault tolerance (ABFT) [28] to detect errors in matrix multiplication related operations. Elliott et al. [19] present selective reliability to provide numerical bounds on anticipated behavior and use this analysis in the design of resilient algorithms [18, 21]. Our work focuses on soft error detection for stencil programs. Application-independent approaches for iterative programs rely on observing the evolution of a value over time to detect anomalies (e.g., AID [17] uses curve fitting, SSD [45] uses support vector machines (SVM) regression, [41] uses a machine learning based approach to build regression models for synthesizing low cost detectors). Gomez and Capello exploits multivariate interpolation in order to detect and correct corruption in stencil application [25]. Xiaoguang [54] presents a *grid sampling* based DMR scheme which determines the sampling points based on the error propagation pattern in the grid.

Gamell considers local recovery from fail-stop errors affecting stencil programs [23]. Fang et al. [22] analytically model application overhead of recovery from detected soft errors via localized recovery. Our approach can complement such recovery algorithms via efficient error detection.

9 CONCLUSIONS AND FUTURE WORK

In this paper, we present FPDETECT, an approach to provide error detection that covers both logical bugs and soft errors in the data space of stencil computations. Schemes comparable to FPDETECT have been observed to generate false positives, incur higher overheads, or not provide similar rigorous guarantees. We report FPDETECT's overheads for different thread counts as well as its performance in conjunction with polyhedral optimizations of the code over for various user-defined precision values. We believe that FPDETECT can be used as part of a holistic error detection system (e.g., involving cross-layer concerns [11]) in which the most impactful of errors affecting stencil programs can be protected.

As future work, we will investigate the use of FPDETECT for runtime precision profiling, given that developers often use high precision as a safety net for floating point errors, which may be wasteful in many cases. FPDETECT's evaluation units are uniquely designed to allow it to serve as a very close proxy to real values at runtime. Thus it can help profile runtime precision requirements. In addition to re-instating confidence in the evolving results, this approach may enable the user to dynamically tune the working precision based on the stability of the evolving results. To this end, we have prototyped a machine learning model built on profiled simulation data that attempts to predict the minimum precision around a rectangular region centered around a point for which FPDETECT's evaluation unit was instantiated. Current results show encouraging trends with prediction accuracies within 2 precision bits. Some of our ongoing work aims to leverage this information in tuning simulation parameters for improved performance.

REFERENCES

- [1] 2008. IEEE Standard for Floating-Point Arithmetic. *IEEE Std 754-2008* (Aug 2008), 1–70. <https://doi.org/10.1109/IEEESTD.2008.4610935>
- [2] George A. Articolo. 2009. *Partial Differential Equations & Boundary Value Problems with Maple, Second Edition* (2nd ed.). Academic Press, Inc., Orlando, FL, USA.
- [3] Wenlei Bao, Sriram Krishnamoorthy, Louis-Noël Pouchet, Fabrice Rastello, and P. Sadayappan. 2016. PolyCheck: dynamic verification of iteration space transformations on affine programs. In *POPL*. 539–554.
- [4] R. Baumann. 2005. Soft errors in advanced computer systems. *IEEE Design Test of Computers* 22, 3 (May 2005), 258–266. <https://doi.org/10.1109/MDT.2005.69>
- [5] Sylvie Boldo and Jean-Christophe Filliâtre. 2007. Formal Verification of Floating-Point Programs. In *ARITH*. 187–194.
- [6] Sylvie Boldo and Thi Minh Nguyen. 2011. Proofs of Numerical Programs when the Compiler Optimizes. *Innov. Syst. Softw. Eng.* 7, 2 (June 2011), 151–160. <https://doi.org/10.1007/s11334-011-0151-6>
- [7] Uday Bondhugula, Muthu Baskaran, Sriram Krishnamoorthy, J. Ramanujam, A. Rountev, and P. Sadayappan. 2008. Automatic Transformations for Communication-Minimized Parallelization and Locality Optimization in the Polyhedral Model. In *ETAPS CC*.
- [8] Uday Bondhugula, Albert Hartono, J. Ramanujam, and P. Sadayappan. 2008. A Practical Automatic Polyhedral Parallelizer and Locality Optimizer. In *Proceedings of the 29th ACM SIGPLAN Conference on Programming Language Design and Implementation (PLDI '08)*. ACM, New York, NY, USA, 101–113. <https://doi.org/10.1145/1375581.1375595>
- [9] S. Borkar. 2005. Designing reliable systems from unreliable components: the challenges of transistor variability and degradation. *IEEE Micro* 25, 6 (Nov 2005), 10–16. <https://doi.org/10.1109/MM.2005.110>
- [10] Michael Carbin, Sasa Misailovic, and Martin C. Rinard. 2013. Verifying quantitative reliability for programs that execute on unreliable hardware. In *OOPSLA*. 33–52.
- [11] Eric Cheng, Shahrzad Mirkhani, Lukasz G. Szafaryn, Chen-Yong Cher, Hyungmin Cho, Kevin Skadron, Mircea R. Stan, Klas Lilja, Jacob A. Abraham, Pradip Bose, and Subhasish Mitra. 2018. Tolerating Soft Errors in Processor Cores Using CLEAR (Cross-Layer Exploration for Architecting Resilience). *IEEE Trans. on CAD of Integrated Circuits and Systems* 37, 9 (2018), 1839–1852. <https://doi.org/10.1109/TCAD.2017.2752705>

- [12] Wei-Fan Chiang, Mark Baranowski, Ian Briggs, Alexey Solovyev, Ganesh Gopalakrishnan, and Zvonimir Rakamaric. 2017. Rigorous floating-point mixed-precision tuning. In *POPL*. 300–315.
- [13] Eva Darulova and Viktor Kuncak. 2014. Sound compilation of reals. In *POPL*. 235–248.
- [14] Eva Darulova and Viktor Kuncak. 2017. Towards a Compiler for Reals. *ACM Trans. Program. Lang. Syst.* 39, 2, Article 8 (March 2017), 28 pages.
- [15] Marc Daumas, Guillaume Melquiond, and César A. Muñoz. 2005. Guaranteed Proofs Using Interval Arithmetic. In *ARITH*. 188–195.
- [16] Luiz Henrique de Figueiredo and Jorge Stolfi. 2004. Affine Arithmetic: Concepts and Applications. *Numerical Algorithms* 37, 1 (01 Dec 2004), 147–158.
- [17] Sheng Di and Franck Cappello. 2016. Adaptive Impact-Driven Detection of Silent Data Corruption for HPC Applications. *TPDS* 27, 10 (2016), 2809–2823.
- [18] James Elliott, Mark Hoemmen, and Frank Mueller. 2014. Evaluating the Impact of SDC on the GMRES Iterative Solver. In *IPDPS*. 1193–1202.
- [19] James Elliott, Mark Hoemmen, and Frank Mueller. 2014. Resilience in Numerical Methods: A Position on Fault Models and Methodologies. *CoRR* abs/1401.3013 (2014).
- [20] James Elliott, Mark Hoemmen, and Frank Mueller. 2015. A Numerical Soft Fault Model for Iterative Linear Solvers. In *HPDC*. 271–274.
- [21] James Elliott, Mark Hoemmen, and Frank Mueller. 2016. Exploiting data representation for fault tolerance. *J. Comput. Science* 14 (2016), 51–60.
- [22] Aiman Fang, Aurélien Cavelan, Yves Robert, and Andrew A. Chien. 2017. Resilience for Stencil Computations with Latent Errors. In *ICPP*. 581–590.
- [23] Marc Gamell, Keita Teranishi, Michael A. Heroux, Jackson Mayo, Hemanth Kolla, Jacqueline Chen, and Manish Parashar. 2015. Local recovery and failure masking for stencil-based applications at extreme scales. In *SC*. 70:1–70:12.
- [24] David Goldberg. 1991. What Every Computer Scientist Should Know About Floating-point Arithmetic. *ACM Comput. Surv.* 23, 1 (March 1991), 5–48.
- [25] L. A. B. Gomez and F. Cappello. 2015. Detecting and Correcting Data Corruption in Stencil Applications through Multivariate Interpolation. In *2015 IEEE International Conference on Cluster Computing*. 595–602. <https://doi.org/10.1109/CLUSTER.2015.108>
- [26] John L. Hennessy and David A. Patterson. 2019. A New Golden Age for Computer Architecture. *Commun. ACM* 62, 2 (Jan. 2019), 48–60. <https://doi.org/10.1145/3282307>
- [27] Nicholas J. Higham. 2002. *Accuracy and Stability of Numerical Algorithms* (second ed.). Society for Industrial and Applied Mathematics. <https://doi.org/10.1137/1.9780898718027> arXiv:<https://epubs.siam.org/doi/pdf/10.1137/1.9780898718027>
- [28] Kuang-Hua Huang and Jacob A. Abraham. 1984. Algorithm-Based Fault Tolerance for Matrix Operations. *IEEE Trans. Computers* 33, 6 (1984), 518–528.
- [29] Padma Jayaraman and Ranjani Parthasarathi. 2017. A Survey on Post-Silicon Functional Validation for Multicore Architectures. *ACM Comput. Surv.* 50, 4, Article 61 (Aug. 2017), 30 pages. <https://doi.org/10.1145/3107615>
- [30] William Kahan. 1996. IEEE standard 754 for binary floating-point arithmetic. *Lecture Notes on the Status of IEEE 754*, 94720-1776 (1996), 11.
- [31] Gokcen Kestor, Burcu Ozcelik Mutlu, Joseph Manzano, Omer Subasi, Osman Unsal, and Sriram Krishnamoorthy. 2018. Comparative Analysis of Soft-error Detection Strategies: A Case Study with Iterative Methods. In *Proceedings of the 15th ACM International Conference on Computing Frontiers (CF '18)*. ACM, New York, NY, USA, 173–182. <https://doi.org/10.1145/3203217.3203240>
- [32] Walter Krämer. 1997. A Priori Worst-Case Error Bounds for Floating-Point Computations. In *ARITH*. 64.
- [33] Qingrui Liu, Changhee Jung, Dongyoon Lee, and Devesh Tiwari. 2015. Clover: Compiler Directed Lightweight Soft Error Resilience. *SIGPLAN Not.* 50, 5, Article 2 (June 2015), 10 pages. <https://doi.org/10.1145/2808704.2754959>
- [34] Victor Magron, George Constantinides, and Alastair Donaldson. 2017. Certified Roundoff Error Bounds Using Semidefinite Programming. *ACM Trans. Math. Softw.* 43, 4, Article 34 (Jan. 2017), 31 pages. <https://doi.org/10.1145/3015465>
- [35] Sasa Misailovic, Michael Carbin, Sara Achour, Zichao Qi, and Martin C. Rinard. 2014. Chisel: reliability- and accuracy-aware optimization of approximate computational kernels. In *OOPSLA*. 309–328.
- [36] Jean-Michel Muller, Nicolas Brisebarre, Florent de Dinechin, Claude-Pierre Jeannerod, Vincent Lefèvre, Guillaume Melquiond, Nathalie Revol, Damien Stehlé, and Serge Torres. 2009. *Handbook of Floating-Point Arithmetic* (1st ed.). Birkhäuser Basel.
- [37] H. Quinn and P. Graham. 2005. Terrestrial-based radiation upsets: a cautionary tale. In *13th Annual IEEE Symposium on Field-Programmable Custom Computing Machines (FCCM'05)*. 193–202. <https://doi.org/10.1109/FCCM.2005.61>
- [38] Jude A. Rivers, Meeta S. Gupta, Jeonghee Shin, Prabhakar N. Kudva, and Pradip Bose. 2011. Error Tolerance in Server Class Processors. in *IEEE Transactions on Computer-Aided Design of Integrated Circuits and Systems (CADICS)* 30, 7

- (2011), 945–959.
- [39] Markus Schordan, Pei-Hung Lin, Daniel J. Quinlan, and Louis-Noël Pouchet. 2014. Verification of Polyhedral Optimizations with Constant Loop Bounds in Finite State Space Computations. In *ISoLA*. 493–508.
 - [40] N. Seifert. 2010. *Radiation-induced Soft Error: A Chip-level Modeling*. now. <https://ieeexplore.ieee.org/document/8187026>
 - [41] Veronica Sharma, G. Gopalkrishnan, and Greg Bronevetsky. 2015. Detecting Soft Errors in Stencil based Computations.
 - [42] Marc Snir, Robert W. Wisniewski, Jacob A. Abraham, Sarita V. Adve, Saurabh Bagchi, et al. 2014. Addressing failures in exascale computing. *IJHPCA* 28, 2 (2014), 129–173.
 - [43] Alexey Solovyev, Marek S. Baranowski, Ian Briggs, Charles Jacobsen, Zvonimir Rakamaric, and Ganesh Gopalakrishnan. 2019. Rigorous Estimation of Floating-Point Round-Off Errors with Symbolic Taylor Expansions. *ACM Trans. Program. Lang. Syst.* 41, 1 (2019), 2:1–2:39. <https://dl.acm.org/citation.cfm?id=3230733>
 - [44] Omer Subasi, Sheng Di, Prasanna Balaprakash, Osman S. Unsal, Jesús Labarta, Adrián Cristal, Sriram Krishnamoorthy, and Franck Cappello. 2017. MACORD: Online Adaptive Machine Learning Framework for Silent Error Detection. In *CLUSTER*. 717–724.
 - [45] Omer Subasi, Sheng Di, Leonardo Bautista-Gomez, Prasanna Balaprakash, Osman S. Unsal, Jesús Labarta, Adrián Cristal, and Franck Cappello. 2016. Spatial Support Vector Regression to Detect Silent Errors in the Exascale Era. In *CCGrid*. 413–424.
 - [46] Omer Subasi and Sriram Krishnamoorthy. 2017. A Gaussian Process Approach for Effective Soft Error Detection. In *CLUSTER*. 608–612.
 - [47] Yuan Tang, Rezaul Alam Chowdhury, Bradley C Kuzmaul, Chi-Keung Luk, and Charles E Leiserson. 2011. The pochoir stencil compiler. In *SPAA*. 117–128.
 - [48] Dingwen Tao, Shuaiwen Leon Song, Sriram Krishnamoorthy, Panruo Wu, Xin Liang, Eddy Z. Zhang, Darren J. Kerbyson, and Zizhong Chen. 2016. New-Sum: A Novel Online ABFT Scheme For General Iterative Methods. In *HPDC*. 43–55.
 - [49] Devesh Tiwari, Saurabh Gupta, George Gallarno, Jim Rogers, and Don Maxwell. 2015. Reliability Lessons Learned from GPU Experience with the Titan Supercomputer at Oak Ridge Leadership Computing Facility. In *Proceedings of the International Conference for High Performance Computing, Networking, Storage and Analysis (SC '15)*. ACM, New York, NY, USA, Article 38, 12 pages. <https://doi.org/10.1145/2807591.2807666>
 - [50] Ohio State University. [n. d.]. the PolyOpt polyhedral compiler. ([n. d.]). http://hpcrl.cse.ohio-state.edu/wiki/index.php/Polyhedral_Compilation.
 - [51] Sven Verdoolaege, Gerda Janssens, and Maurice Bruynooghe. 2012. Equivalence checking of static affine programs using widening to handle recurrences. *ACM Trans. Program. Lang. Syst.* 34, 3 (2012), 11:1–11:35.
 - [52] Panruo Wu and Zizhong Chen. 2014. FT-ScaLAPACK: correcting soft errors on-line for ScaLAPACK cholesky, QR, and LU factorization routines. In *HPDC*. 49–60.
 - [53] Panruo Wu, Nathan DeBardeleben, Qiang Guan, Sean Blanchard, Jieyang Chen, Dingwen Tao, Xin Liang, Kaiming Ouyang, and Zizhong Chen. 2017. Silent Data Corruption Resilient Two-sided Matrix Factorizations. In *PPoPP*. 415–427.
 - [54] Ren Xiaoguang, Xu Xinhai, Wang Qian, Chen Juan, Wang Miao, and Yang Xuejun. 2015. GS-DMR: Low-overhead soft error detection scheme for stencil-based computation. *Parallel Comput.* 41 (2015), 50 – 65. <https://doi.org/10.1016/j.parco.2014.11.003>
 - [55] Yaqi Zhang, Ralph Nathan, and Daniel J. Sorin. 2015. Reduced Precision Checking to Detect Errors in Floating Point Arithmetic. (2015). [arXiv:cs.NA/1510.01145](https://arxiv.org/abs/1510.01145)

FPDetect : Supporting Material

CONTENTS

Contents	1
A Error Analysis	2
A.1 Floating point basics	2
A.2 Affine Analysis	2
A.3 Arithmetic Operations Using Affine Arithmetic	3
A.4 Affine model for Floating Point	4
A.5 Modeling rounding error in Stencils	5
B Precision Driven Optimizations	9
B.1 Overview	9
B.2 Precision reasoning on operand exponents	10
B.3 Modeling Protected Width (P_w)	11
B.4 Modeling Essential Width (E_w)	13
C Overall Algorithm	14
C.1 Offline algorithm.	14
C.2 Online Detector-Embedded Execution	15
D Software Bug Detection	17
References	21

arXiv:2004.04359v2 [cs.DC] 13 Apr 2020

In this material we provide the detailed proof discussions and the analytical choices made in our tool design. We have highlighted the key results from our work inside the main paper, and present the complete derivation of the concepts here for completeness. The interested reader is encouraged to have a detailed look into the derivations.

We discuss broadly the four major sections. In *Error Analysis* we detail the complete derivation of our affine arithmetic based round-off error analysis to obtain the detector precision. *Precision Driven Optimizations* describes the methodology behind obtaining the **Essential Width** and **Protected Width**. *Overall Algorithm* provides the exact algorithms used for the offline/online split phases. In *software Bug Detection* provide examples of the types of bugs introduced and summary of the Pluto generated code and it's results.

A ERROR ANALYSIS

A.1 Floating point basics

A floating point number system corresponding to a certain radix is a subset of the set of real numbers, and can be expressed as a 5 tuple (β, s, m, e, p) . Here β is the radix or the base of the floating point system. Our work concern with $\beta = 2$, that is the binary floating point system in double precision with $p = 53$. $s \in \{-1, 1\}$ is the sign bit, m is called the significand or mantissa and e is the exponent. There are two types of floating point numbers, the *normal* and the *denormals*, other than the special cases of NaNs and infinities. For the *normal* numbers m lies in the range $1 \leq m < 2$, while for *denormals* the range is $0 \leq m \leq 1$. The denormal range begins after the lowest *normal* number to make a gradual transition towards zero. e is the exponent in the range $-1022 \leq e \leq 1023$. Any such number x_f belonging to the floating point system \mathbb{F} has the value $s \cdot m \cdot 2^e$. If $x \in \mathbb{R}$, then $x_f \in \mathbb{F}$ denotes an element in \mathbb{F} closest to x obtained by applying the rounding operator (\circ) to x .

IEEE754 [1] defines four rounding modes for elementary floating point operations namely rounding towards positive infinity ($\circ_{+\infty}$), towards negative infinity ($\circ_{-\infty}$), towards zero (\circ_0) and to the nearest (\circ_{\cdot}). Every real number x lying in the range of \mathbb{F} can be approximated by an element $x_f \in \mathbb{F}$ with a relative error no larger than the *unit round-off* $\mathbf{u} = \frac{1}{2}\beta^{1-p}$. Here β^{1-p} corresponds to the *unit of least precision (ulp)* for exponent value of 1. We use μ to denote ulp (1), such that $\mu = 2\mathbf{u}$. In our case $\mathbf{u} = 2^{-53}$, and hence $\mu = 2^{-52}$. Hence, for all $\circ \in \{\circ_{+\infty}, \circ_{-\infty}, \circ_0, \circ_{\cdot}\}$, we have the following result

THEOREM A.1. *If $x \in \mathbb{R}$ lies in the range of \mathbb{F} , then*

$$\circ(x) = x(1 + \delta), \quad |\delta| \leq \mathbf{u} = \mu/2 \quad (1)$$

Given two exactly represented floating point numbers x_f and y_f , arithmetic operators $\diamond \in \{+, -, \times\}$ have the following guarantees across for any rounding modes

$$x_f \diamond_f y_f = (x_f \diamond y_f)(1 + \delta), \quad |\delta| \leq 2\mathbf{u} = \mu \quad (2)$$

Thus the computed floating point value post rounding represents an interval $[x_f \diamond y_f \pm |x_f \diamond y_f| 2\mathbf{u}]$ of real numbers, any of which could have produced the computed value. Multiplication operators have a stricter bound of $|\delta| \leq \mathbf{u}$

A.2 Affine Analysis

In Affine Arithmetica (AA) [5], a computed quantity (\hat{x}) is expressed in an affine form over its true value and its accumulated error quantities as shown in equation (3).

$$\hat{x} = x_0 + \sum_{i=1}^n x_i \epsilon_i \quad (3)$$

Here, x_0 is the central value tracking the true value of \hat{x} . The coefficients x_i are finite floating point numbers and the ϵ_i are *formal noise variables* which are unknown until concretized but assumed to lie in the interval $[-1, +1]$. To interpret an affine variable using an equivalent interval notation, the noise variables are concretized to their maximum range obtaining the interval I_x .

$$I_x = [x_0 - rad(\hat{x}), x_0 + rad(\hat{x})]; \quad rad(\hat{x}) = \sum_{i=1}^n |x_i| \quad (4)$$

The real advantage of AA can be seen by deferring the concretization process as far down the computation depth as possible since once concretized, it loses any variable correlation that might be present. Before concretizing, incoming contributions from the same or related noise variables are superposed, hence they can accumulate or cancel based on the sign of the coefficients x_i . For example, when evaluating $(x - x)$, affine arithmetic yields 0, unlike interval analysis where it doubles the interval.

A.3 Arithmetic Operations Using Affine Arithmetic

We define the following three operators to deal with retrieval of noise variables and its coefficients.

- σ : Defines the mapping from an affine variable to its set of noise variables. Thus $\sigma(\hat{x}) = \{\epsilon_i\}_{i=1}^n$.
- $\sigma^{(0)}$: A special σ to retrieve *freshly generated noise variables* at the last stage of compute of \hat{x} . Its purpose is to distinguish between freshly generated noise variables versus the existing ones.
- γ : Defines the mapping from a 2-tuple of (*affine variable, noise variable*) to its corresponding noise coefficient. Thus

$$\gamma(\hat{x}, \epsilon_i) = \begin{cases} x_i; & \epsilon_i \in \sigma(\hat{x}) \\ 0; & \text{otherwise} \end{cases}$$

Based on the definitions for σ and γ , we now define the two affine variables \hat{x} and \hat{y} as

$$\hat{x} = x_0 + \sum_{\epsilon_i \in \sigma(\hat{x})} \gamma(\hat{x}, \epsilon_i) \epsilon_i; \quad \hat{y} = y_0 + \sum_{\epsilon_i \in \sigma(\hat{y})} \gamma(\hat{y}, \epsilon_i) \epsilon_i \quad (5)$$

We consider only, (a) a scalar multiplication and (b) an affine addition for dealing with dot products pertinent to stencil computations.

Scalar Multiplication. Let α denote an exactly represented scalar quantity, then

$$\alpha \hat{x} = \alpha x_0 + \sum_{\epsilon_i \in \sigma(\hat{x})} \alpha \gamma(\hat{x}, \epsilon_i) \epsilon_i \quad (6)$$

Affine Addition. The coefficients of the common noise variables are linearly superposed preserving their correlation, hence coefficients of a common noise variable of equal but opposing sign can cancel out eliminating that noise variable.

$$\begin{aligned} \hat{x} + \hat{y} &= (x_0 + \sum_{\epsilon_i \in \sigma(\hat{x})} \gamma(\hat{x}, \epsilon_i) \epsilon_i) + (y_0 + \sum_{\epsilon_i \in \sigma(\hat{y})} \gamma(\hat{y}, \epsilon_i) \epsilon_i) \\ &= (x_0 + y_0) + \sum_{\substack{\epsilon_i \in \\ \sigma(\hat{x}) \cup \sigma(\hat{y})}} (\gamma(\hat{x}, \epsilon_i) + \gamma(\hat{y}, \epsilon_i)) \epsilon_i + \{\text{higher order terms}\} \end{aligned} \quad (7)$$

Note that the x_i coefficients obtained using γ are finite floating point numbers. Hence during the scaling or superposition operations they incur rounding error as well leading to higher order rounding terms.

A.4 Affine model for Floating Point

Equation (1) shows the relation between a real number $x \in \mathbb{R}$ and its rounded floating point representation, $x_f = \circ(x) \in \mathbb{F}$. We can represent the floating point variable by associating the uncertainty radius with a noise variable as shown in equation (8)

$$\begin{aligned} x_f = \circ(x) &= x(1 + \delta); \quad |\delta| \leq \mathbf{u} \\ &= x + (x\mathbf{u})\epsilon; \quad \epsilon \in [-1, +1] \end{aligned} \quad (8)$$

Let x_f and y_f be two floating point variables represented as in equation (5) such that $x_f = \hat{x}$ and $y_f = \hat{y}$. Instead of the central values being x_0 and y_0 , we replace them by the real number x and y respectively as per the definition of our model.

$$x_f = x + \sum_{\epsilon_i \in \sigma(\hat{x})} \gamma(\hat{x}, \epsilon_i)\epsilon_i; \quad y_f = y + \sum_{\epsilon_i \in \sigma(\hat{y})} \gamma(\hat{y}, \epsilon_i)\epsilon_i \quad (9)$$

Also, let α and β be two exactly represented scalar quantities as before. In this model every floating point operation, $\diamond_f \in \{\circ(+), \circ(-), \circ(\times)\}$ introduces a *fresh noise variable* with coefficients equal to the uncertainty of maximum round-off error introduced by that operation as in (2). We consider two operations specific to the stencil inner product: (1) scaling x_f by an exactly represented scalar α shown in (10), and (2) add or subtract two error-laden FP numbers x_f and y_f as shown in (11)

$$\circ(\alpha \times x_f) = \left(\alpha x + \sum_{\epsilon_i \in \sigma(x_f)} \alpha \gamma(x_f, \epsilon_i)\epsilon_i \right) + ((\alpha x)\boldsymbol{\mu})\epsilon_{new} + \{\text{he}\} \quad (10)$$

$$\begin{aligned} \circ(x_f + y_f) &= (x + y) + \sum_{\epsilon_i \in \sigma(x_f) \cup \sigma(y_f)} \{\gamma(x_f, \epsilon_i) + \gamma(y_f, \epsilon_i)\}\epsilon_i \\ &\quad + ((x + y)\boldsymbol{\mu})\epsilon_{new} + \{\text{he}\} \end{aligned} \quad (11)$$

Observations from equation (10) and (11)

- A new formal noise variable gets introduced, denoted here as ϵ_{new} for every new floating point operation.
- Furthermore, the α scaling operations in (10) or the linear superposition of the coefficients in (11) over the set of union of the noise variables show how the error from previous stages get propagated to future computations. However, these operations are also to be performed in finite precision and hence introduces second order noise variable which we have bracketed out as *higher order error terms*. We choose to ignore second and higher order error terms (that is \mathbf{u}^2 or higher) since they do not substantially affect the analysis until the problem size approaches 2^{53} . Considering higher order noise variables leads to an explosion of new noise variables being produced while not adding significant benefit to the accuracy analysis of the system, we ignore the second order terms.
- If $\epsilon_i \in \sigma(x_f) \cap \sigma(y_f)$, then in the linear superposition considering the affine model we get $(\gamma(x_f, \epsilon_i) + \gamma(y_f, \epsilon_i))$ while when using interval analysis would result in $(|\gamma(x_f, \epsilon_i)| + |\gamma(y_f, \epsilon_i)|)$ which would have been a large over-approximation when there is a mix of addition and cancellation terms.

Generation and Propagation of Errors: Darulova [4] introduces the notion of separating the *generation* and *propagation* of errors. This helps to analyze the effect of each individual formal noise variable separately instead of over-approximating all error terms together as done in interval analysis. We extend its application to stencil codes. Consider a real function f and its floating point version \tilde{f} . The real set of variables is denoted by \mathbf{x} while the rounded off variable set (with error laden terms intrinsically) are denoted as $\tilde{\mathbf{x}}$. Then the total error can be written and decomposed in

the form

$$|f(\mathbf{x}) - \tilde{f}(\tilde{\mathbf{x}})| \leq \overbrace{|f(\mathbf{x}) - f(\tilde{\mathbf{x}})|}^{\text{propagation of errors}} + \overbrace{|f(\tilde{\mathbf{x}}) - \tilde{f}(\tilde{\mathbf{x}})|}^{\text{Freshly generated errors}} \quad (12)$$

The first term essentially represents the contribution of the initial error in the input to the output. Thus each input variable associates with itself a propagation factor by which error on the input gets propagated to the output. The propagation factor essentially characterizes the rate at which the output changes for some delta change in the input. Here the delta change in the input is the round-off term associated with the error laden input variable. Thus the propagation factor essentially depends on the derivative of the function with respect to the input points.

Let K_i denote the propagation factor for variable x_i and $\sigma(x_i)$ denotes the set of noise variables existing at x_i as part of incoming error. Then

$$|f(\mathbf{x}) - f(\tilde{\mathbf{x}})| \leq \sum_{i=1}^m K_i \left(\sum_{\epsilon_i \in \sigma(x_i)} \gamma(x_i, \epsilon_i) \epsilon_i \right); \quad \text{where, } K_i = \sup_{w_i \in \tilde{\mathbf{x}}} \left| \frac{\partial f}{\partial w_i} \right| \quad (13)$$

Evaluating K_i factors is easy to visualize once the computational graph is available as shown in Figure 1.

As a simple illustration, consider a single step iteration of a 1-d 3-point stencil with stencil coefficients $\{c_1, c_2, c_3\}$ centered around x_2 to evaluate x_2 for the next time step, denoted here as S in Figure 1. Thus the computational graph evaluates $S = ((c_1 \times x_1) + (c_2 \times x_2)) + (c_3 \times x_3)$. If ϵ' is a noise variable belonging to $\sigma(x_1)$, then the error contribution's propagation at S will be

$$\begin{aligned} \gamma(x_1, \epsilon') \cdot K_{x_1} &= \gamma(x_1, \epsilon') \cdot \left| \frac{dS}{dx_1} \right| = \gamma(x_1, \epsilon') \cdot \left| \frac{dS}{dS} \cdot \frac{dS}{dq} \cdot \frac{dq}{dz_1} \cdot \frac{dz_1}{dx_1} \right| \\ &= \gamma(x_1, \epsilon') \cdot 1 \cdot 1 \cdot 1 \cdot c_1 = \gamma(x_1, \epsilon') \cdot c_1 \end{aligned} \quad (14)$$

Thus for all such $\epsilon' \in \sigma(x_1)$, the $\gamma(x_i, \epsilon')$ gets propagated by c_1 . Similarly for x_2 and x_3 .

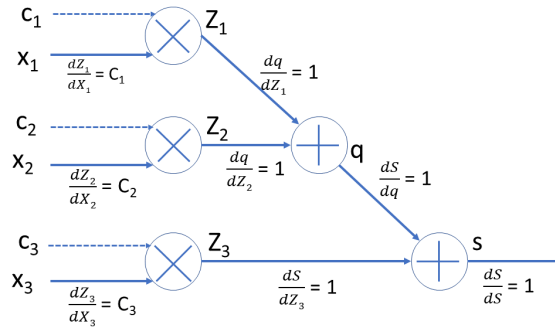


Fig. 1. Computational graph with highlighted derivatives for 1 step of a 1-d 3-point stencil

A.5 Modeling rounding error in Stencils

Stencil applications modeling real world partial differential equations in fluids, combustion, cosmology and other computing areas are required to deal with multiple physical quantities. For example, when modeling electromagnetic fields with finite difference time domain methods, there are atleast two arrays corresponding to the electric and magnetic field whose updates are intrinsically dependent on both arrays. To address more complicated structures, we introduce the notion of multiple array updates. Suppose, every contribution depends on contributions from N participating arrays. We denote the iterative stencil update rule by f_s^m which associates the stencil update function

to the domain of grid points, \vec{x} , and the array being updated. Equation (15) shows the *single step update rule* for updating location $A_u[\vec{x},t]$, that is location \vec{x} of array A_u for time step t

$$f_s^1(\vec{x}, t, A_u) = \sum_{v=1}^N \sum_{\vec{i}=-\vec{w}}^{\vec{w}} c_{(u,v,\vec{i},1)} \times A_v[\vec{x} + \vec{i}, t - 1] \quad (15)$$

where, $c_{(u,v,\vec{i},1)}$ denotes the contributing coefficient from array A_v to array A_u from the location at an offset \vec{i} from \vec{x} over a single step. The iterator \vec{i} loops over the stencil-width \vec{w} in the neighborhood of the point. If we unroll f_s^1 over k iterations symbolically and reassociate the coefficients, we obtain a *real-space equivalent* ($=_{real}$) *update rule to compute directly over k iterations*. We define the *direct update rule* by f_d^k as:

$$f_d^k(\vec{x}, t, A_u) = \sum_{v=1}^N \sum_{\vec{i}=-k\vec{w}}^{k\vec{w}} c_{(u,v,\vec{i},k)} \times A_v[\vec{x} + \vec{i}, t - k] \quad (16)$$

such that $A_u[\vec{x},t] =_{real} f_d^k(\vec{x}, t, A_u)$. Note that as we unroll over k steps, the stencil width proportionally extends over $k\vec{w}$ neighborhood of the location \vec{x} .

We use the *multi-step update rule* as our *alternative evaluation strategy* for a detector located at a point $A_u[\vec{x},t_0 + T]$ using values from a baseline at $t = t_0$ as modeled by $f_d^T(\vec{x}, t_0 + T, A_u)$ and refer to it as **direct evaluation**. First, we determine the effective path contribution from each point on the baseline $t=t_0$ towards $A_u[\vec{x},t_0 + T]$ that fall inside its dependence cone and then perform a dot-product of these coefficients with the corresponding data points from the baseline.

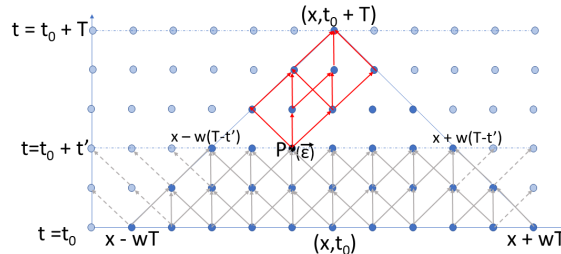


Fig. 2. Error propagation from point $(x-1, t_0+t')$ to (x, t_0+T) (1-d stencil)

Figure 2 shows the dependence cone and the data value flow paths when evaluating a stencil point at (t_0+T, \vec{x}) from a baseline at $t=t_0$ for a single array 1-d 3-point stencil. Evaluation of each node of this stencil comprise of three multiplications and two additions, same as the computational flow graph shown in fig 1. In total five operations per node results in 5 fresh noise variable generated per node. Thus the space complexity is linear in the number of data points. For a d-dimensional problem with N-arrays and T-step detector model, the space complexity for the noise variables will be $O(NT^d)$. For notation, we always consider the update towards array A_u , but the same holds for all participating arrays. Consider a point \vec{P} located within the dependence cone, t' steps in the future from the baseline and equivalently $(T - t')$ in the past from the point $(t_0 + T, \vec{x})$. The value at \vec{P} is obtained after executing the iterative stencil over t' steps, that is $f_s^{t'}(\vec{P}, t_0 + t', A_u)$. $\sigma(A_u[\vec{P}, t_0+T])$ denotes the set of noise variables at \vec{P} for array A_u . It comprises of the set of incoming noise variables already generated (*propagation of errors*) before reaching the stage of evaluation of $f_s^1(\vec{P}, t_0 + t' - 1, A_u)$ and the new noise variables generated due to round-off from its execution.

Thus, we have

$$\sigma(A_u[\vec{P}, t_0 + t']) = \overbrace{\bigcup_{v=1}^N \left(\bigcup_{\vec{i}=-\vec{w}}^{\vec{w}} \sigma(A_v[\vec{P} + \vec{i}, t_0 + t' - 1]) \right)}^{\text{propagation of incoming errors generated before } t + t'} \cup \underbrace{\sigma^{(0)}(A_u[\vec{P}, t_0 + t'])}_{\text{freshly generated errors at } t + t'} \quad (17)$$

In equation (17), the first term on the rhs indicate the propagation of existing errors before reaching the compute stage of \vec{P} . The second term of the union retrieves the freshly generated noise variables at \vec{P} using the operator $\sigma^{(0)}$.

Once a noise variable is freshly generated at \vec{P} , its magnitude is scaled by the effective path contribution from \vec{P} to the destination $A_u[\vec{x}, t_0 + T]$ which in the derivative form can be summarized as

$$\left| \frac{dA_u[\vec{x}, t_0 + T]}{dA_v[\vec{P}, t_0 + t']} \right| = c_{(u, v, \vec{x} - \vec{P}, T - t')} \quad (18)$$

depending on which participating array \vec{P} belongs to for a multi-array update. Thus, instead of dynamically propagating the noise variables at every step, we associate a set of fresh noise variables with each compute node of the CFG, and then scale them directly with the pre-computed coefficients of equation (18). For an intermediate time tile at $t = t_0 + t'$, let $E_{u, v}^{t'}$ denote the total error contribution for the new noise variables at $(t_0 + t')$ due to A_v contributing towards A_u . Then we have

$$E_{u, v}^{t'} = \sum_{\substack{\vec{i} = \\ -\vec{w}(T-t')}}^{\vec{w}(T-t')} \left(\sum_{\substack{\epsilon_i \in \\ \sigma^{(0)}(\vec{P}_{(t', \vec{i})})}} \left| \overbrace{\gamma(\vec{P}_{(t', \vec{i})}, \epsilon_i)}^{\text{noise coefficient}} \times \underbrace{c_{(u, v, \vec{i}, T-t')}}_{\text{Propagating coefficient}} \right| \right) \quad (19)$$

where, $\vec{P}_{(t', \vec{i})} = A_v[\vec{x} + \vec{i}, t_0 + t']$. $E_{u, v}^{t'}$ needs to be summed over all the participating arrays that contribute to A_u to obtain the total error term at $t_0 + t'$. To find the total error generated over T steps, we need to sum for all the intermediate t' tiles. Then the total error (T_E) and the relative error (R_E) in the evaluation of $A_u[\vec{x}, t_0 + T]$ are:

$$T_E(A_u[\vec{x}, t_0 + T]) = \sum_{t'=0}^T \left(\sum_{v=1}^N E_{u, v}^{t'} \right) \quad (20)$$

$$R_E(A_u[\vec{x}, t_0 + T]) = \left| \frac{T_E(A_u[\vec{x}, t_0 + T])}{f_d^T(\vec{x}, t_0 + T, A_u)} \right|$$

The relative error measure normalizes the total error by the actual stencil value at that point (ideally the exact real value) hence providing a quantification about how severe the encountered loss is with respect to the actual operating data. Note that when normalizing, the denominator used detector evaluation, f_d^T , and not the stencil's iterated value. In theory, we must normalize by the ideal **real** value but in practice we have to compute in finite precision. However, our direct evaluation is designed to be a very close proxy to real evaluation since parts of it can be exercised at very high precision.

Iterated vs direct loss. Evaluating equation (20) for all $(\vec{x} + \vec{i}, t_0)$ belonging to a bounded input interval $[I_l, I_u]$ derives the relative error for the iterated evaluation of the stencil denoted by R_s . To evaluate the error loss for the direct evaluation, we start from $(\vec{x}, t_0 + T)$ and do a back propagation to compute the coefficient set for f_d^T , followed by a f_d^T evaluation on the input data set bounded in the interval $[I_l, I_u]$. Since, f_d^T computes a large dot product that can introduce significant round off

error, we deploy Kahan’s algorithm [6] for the additive portion of f_d^T , which is computationally more expensive but more precision-preserving summation algorithm. Let the relative error term evaluated for the direct evaluation be R_d . The precision of value computed using direct evaluation need not be any greater than that produced by the iterative stencil.

$$\text{bits preserved}_T = (dp)_T = p - \log_2(\max(R_s, R_d)) \quad (21)$$

Equation (21) evaluates the minimum matching precision between the iterated and direct evaluation schemes over T-steps that survives the loss due to round-off error. This is denoted by **detector precision (dp)**, and represents the maximum precision that can potentially be guaranteed by our detection strategy. Note that our error analysis is conservative in its treatment of input values, and might not capture the maximum precision preserved by a specific set of input values. On the other hand, it provides a rigorous detection guarantee and attempts to minimize total cost in providing that guarantee.

B PRECISION DRIVEN OPTIMIZATIONS

In the main paper we discuss the precision driven optimization techniques employed to reduce the detector computation cost while still guaranteeing the necessary quality detection. The concepts of **Essential Width** and **Protected Width** were introduced briefly with discussions on how they help the optimization process. Here, we delve into further details of these concepts beginning with an intuitive description followed by formalization of the concepts.

B.1 Overview

To simplify the intricacies of the methodologies of *FPDetect*, we begin with a simple one dimensional heat equation description represented in the continuous domain as

$$\begin{aligned} \frac{\partial u}{\partial t} &= \nabla^2 u(x), \quad x \in \Omega \times (0, T] \\ u(x) &= u_D, \quad x \in \partial\Omega \times (0, T] \quad (\text{Dirichlet Boundary Conditions}) \\ u &= u_0(x), \quad t = 0; \quad (\text{Initial Conditions}) \end{aligned} \quad (22)$$

where $u(x)$ corresponds to the exact solution, Ω is the solution domain and $\partial\Omega$ corresponds to the boundary points of the domain. An explicit finite difference solution of (22) is expressed as

$$u_i^{n+1} = \alpha \frac{\Delta t}{\Delta x} u_{i-1}^n + (1 - 2\alpha \frac{\Delta t}{\Delta x}) u_i^n + \alpha \frac{\Delta t}{\Delta x} u_{i+1}^n \quad (23)$$

Here u_i^n is corresponds to the i 'th discretized point during the time iteration n . Thus neighbouring points from the n 'th iteration are used to update a point during its next iteration. The correct choice of the discretization parameters constitute the amount of contribution received from the neighbouring elements in the evolution of a stencil. We consider the following coefficients only for demonstrating the methodologies. Let A denote the one dimensional grid on which $u(x)$ is discretized into $(N+1)$ points including the boundaries. With a set of chosen coefficients conforming to the discretization and stability criterions, a common 1d heat equation form is written as

$$A[x, t + 1] = 0.25 * A[x - 1, t] + 0.5 * A[x, t] + 0.25 * A[x + 1, t] \quad (24)$$

On the rhs of (24) one can further expand by replacing them using points from step $(t - 1)$ and so on. Notice that the offset dependence around i for one iteration in this case is $\{-1, 0, +1\}$, while when unrolled for 2 steps it will be $\{-2, -1, 0, 1, 2\}$ and so on. Let Set_k denote the offset set corresponding to the k 'th unroll. For our example, if we unroll this way, we can see the evolution pattern in the corresponding coefficients as shown in Table 1.

Table 1. Evolution of Coefficient values as we unroll the stencil

Set Number	Coefficients at Offsets							
	offset index \rightarrow	-3	-2	-1	0	1	2	3
Set_1		0	0	0.25	0.5	0.25	0	0
Set_2		0	0.0625	0.25	0.375	0.25	0.0625	0
Set_3		0.015625	0.09375	0.234375	0.3125	0.234375	0.09375	0.015625

While our direct evaluation method by leap-frogging Tsteps is equivalent in the real space, it is still subject to round off error accumulation due to the non compositional nature of floating point numbers. *FPDetect* tries to find the upper bound on the minimum matching precision between the stencil and the direct evaluation executions for a given interval range. using the methods described in section A.5. We call this the detector precision (dp_T).

Given we obtain this bound on the precision to check at the detector, it opens up the possibility of driving optimizations constrained by dp_T . The Set_k values show that as we increase k , the set

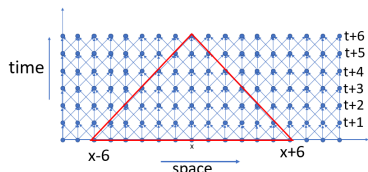


Fig. 3. Simplified 1D stencil over 6 time steps

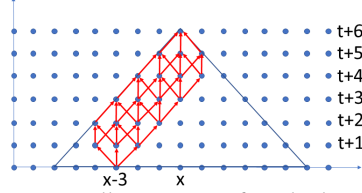


Fig. 4. Illustration of path dominance

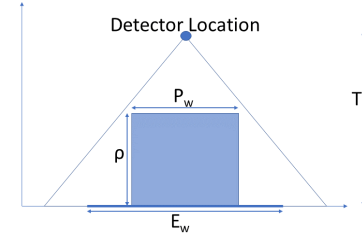


Fig. 5. Essential (E_w) and protected widths (P_w)

of points required in the offset to compute the detector increases. Furthermore, the points at the edges of these dependence sets have reduced contributions to the compute than the interior points. This is due to a combination of associated primary coefficients due to the discretization process and the phenomenon of *path dominance*. We do not consider discretization effects and assume the discretized numerics are designed to be stable including the method error. However, we consider the effect of *path dominance* as shown in fig 4 by the highlighted path contribution.

Essentially, points at the boundary of the cone have lesser path contributions than the interior ones. Notice that when computing in infinite precision we require computing over the entire dependence set to obtain the exact real value. However in finite precision, we have already trimmed our expectation of the preserved accuracy at the detector location by dp_T . For example, when computing in double precision with $p = 53$ bits, *FPDetect* says a detector precision of 45 bits can be matched between the stencil and the detector over 64 iterations for the one dimensional heat example. Hence, points in the dependence set that do not possess sufficiently strong contributing coefficients to affect the detector within 45 bits are good candidates to be **trimmed away** from the detector's dependence set for the evaluation. Thus, instead of the offset being $\{-64, -63, \dots, 0, \dots, 63, 64\}$ will become say $\{-40, -39, \dots, 0, \dots, 39, 40\}$ based on the analysis presented later. We carve out an **essential width** (E_w) out of the full dependence set. This process introduces **controlled approximations** to the detector compute process while still retaining the detector precision bound. Fig 5 shows a representative E_w for a detector.

Furthermore, each point in a detectors dependence cone, contribute to the detector a varying amount of precision. We provide the user with a parametric knob called the **user defined precision (udp)** that lets the user choose how many bits they want to be preserved for fractions of the computation space. For example, suppose the user selects $udp = 20$ bits. In our example, with $dp_{64} = 45$ at the detector, *FPDetect* finds the **minimal set of points which contribute atleast 20 bits of precision to retain 45 bits of precision at the detector**. Thus any mismatch beyond dp_{64} at the detector implies atleast one or more of the points in this minimal set of points been affected. This forms the basis of *FPDetect*'s protection mechanism and this minimal set of points conforming to the udp protection guarantee is called **Protected Width** P_w . Fig 5 shows a representative P_w tile for the given detector. Next we discuss how the E_w and P_w are obtained by detailing the interactions between operating floating point numbers.

B.2 Precision reasoning on operand exponents

In section ??, we denote a floating point number as a 5-tuple (β, s, m, e, p) . For a given radix, $\beta (= 2)$ and a fixed working precision $p (= 53)$ we can represent a number in this system using the 3-tuple of (s, m, e) . Let $a = (s_a, m_a, e_a)$ and $b = (s_b, m_b, e_b)$ be two such floating point numbers under a fixed β and p floating point system. We define a **distance metric (d)**, that quantifies the relative distance of the binades¹ in which the two floating point numbers are represented.

$$d_{ab} = |e_a - e_b| \quad (25)$$

¹A binade is a set of binary floating-point values that all have the same sign and exponent. The distance between successive members belonging to the same binade are equal to the ulp of that binade

Let S_{ab} denote the summation of these two floating point numbers

$$S_{ab} = \circ(a + b) = \circ((s_a, m_a, e_a) + (s_b, m_b, e_b))$$

For floating point addition/subtraction, the two operands are adjusted to bring them in the same binade and then binary addition/subtraction takes effect between the mantissa components followed by rounding. If $e_a > e_b$, then to evaluate S_{ab} , m_b must be shifted by d_{ab} bits to its lsb implying d_{ab} bits of m_b are lost. In other words, in the system with working precision p , only $(p - d_{ab})$ bits of m_b take part in the binary addition to determine the final outcome of S_{ab} . Likewise, if $e_b > e_a$, then m_a shifts by d_{ab} bits towards its lsb.

B.3 Modeling Protected Width (P_w)

Suppose a and b , instead of being two floating point numbers, belongs to an interval such that

$$a \in [a_l, a_u]; \quad b \in [b_l, b_u]$$

where the subscripts l and u denote the lower and upper bounds respectively. We can further break down the floating point representations of the intervals bounds in terms of the 3-tuple expressions as

$$[a_l, a_u] = [(s_a, m_a, e_a), (\bar{s}_a, \bar{m}_a, \bar{e}_a)]; \quad [b_l, b_u] = [(s_b, m_b, e_b), (\bar{s}_b, \bar{m}_b, \bar{e}_b)];$$

To quantify the **minimal possible influence** a has on the summation S_{ab} , we need to find the distance of the exponents between the maxima of b and the minima of a . Hence, the **minimal number of precision bits** (\mathcal{P}_a) of a that part take in the summation for the resulting p precision bits can be quantified as in equation (26) where p is the working precision of the system.

$$\mathcal{P}_a = \begin{cases} p - (\bar{e}_b - e_a) & : (\bar{e}_b - e_a) > 0 \\ p & : (\bar{e}_b - e_a) \leq 0 \end{cases} \quad (26)$$

$$\mathcal{P}_a = p - \max(0, (\bar{e}_b - e_a))$$

Similarly, we can quantify the **minimal possible influence** b has on the S_{ab} as

$$\mathcal{P}_b = p - \max(0, (\bar{e}_a - e_b)) \quad (27)$$

We will next show how to extend the analysis from two points to a set of points. *FPDetect* works by synthesizing detectors for the expected ranges of binades that the stencil computation may begin with. A T -step detector's support comprises of $(2 * T * \vec{w} + 1)$ points centered around a grid location \vec{x} , that is the points in the set $X_D = [\vec{x} - \vec{w}T, \vec{x} + \vec{w}T]$, where \vec{w} represents the footprint of one iteration of the stencil expressed as a vector to include higher dimensional spaces. Each point x_i in X_D belongs to the tightest encompassing interval I . Upon multiplying each x_i by their respective T -step coefficients, c_i , generates separate intervals for each individual product term denotes as

$$[y_i, \bar{y}_i] = [\min(c_i x_i, c_i \bar{x}_i), \max(c_i x_i, c_i \bar{x}_i)]$$

This results in a new set of N points, $Y = [y_1, y_2, \dots, y_N]$, where $N = (2T\vec{w} + 1)$. Thus, we are now extending our *precision influence* analysis from two points to a larger set of N points each belonging to separate intervals. Let S_Y denote the summation of the points in Y over the respective intervals, then

$$\begin{aligned} S_Y &= \sum_{j=1}^N y_j = \sum_{j=1}^N [y_j, \bar{y}_j] \\ &= [S_Y, \bar{S}_Y] \end{aligned} \quad (28)$$

To analyze the minimal contribution of point y_i , we need to compare its contribution with respect to the maximal contribution from all the remaining points over that interval. Let $S_{Y \setminus i}$ denote the partial sum over all points in Y excluding y_i .

$$\begin{aligned} S_{Y \setminus i} &= \sum_{\substack{j=1 \\ i \neq j}}^N y_j \\ &= [\underline{S_{Y \setminus i}}, \overline{S_{Y \setminus i}}] \end{aligned} \quad (29)$$

We redefine the distance metric from equation (25) corresponding to point y_i as $d_{\max}(y_i)$ to be distance between the exponent of the upper bound of $S_{Y \setminus i}$ and the exponent of the lower bound of y_i such that

$$d_{\max}(y_i) = \max(0, \exp(\overline{S_{Y \setminus i}}) - \exp(\underline{y_i})) \quad (30)$$

Then the minimal precision contribution of point y_i to the final sum, S_Y , is computed upto p precision bits will be expressed as

$$\text{minContrib}_p(y_i, S_Y) = p - d_{\max}(y_i)$$

Our bound of correctness of p precision bits holds upto the detector precision, dp_T , for the error analysis of a T-step model of the detector. Hence, we have

$$\text{minContrib}_{dp_T}(y_i, S_Y) = dp_T - d_{\max}(y_i) \quad (31)$$

Equation (31) evaluates the minimal precision of each point in Y that affects S_Y within dp_T bits of precision. This now enables us to partition the set Y based on a **user defined precision (udp)** that the user selects for protection guarantees. Let Y_{udp} denote the set of points in Y whose contribution to S_Y is atleast udp precision. We can define such a set as

$$Y_{udp} = [y_i : \text{minContrib}_{dp_T}(y_i, S_Y) \geq udp, \quad y_i \in Y] \quad (32)$$

The most significant udp bits of precision of each point inside Y_{udp} is then protected if S_Y is evaluated correctly to dp_T bits of precision. The set Y_{udp} forms the building block for obtaining the **Protected Width** (P_w) parameter.

In our stencil model, for a detector placed at $A_u[\vec{x}, t_0+T]$, we define **Protected Width** ($P_w(T, \rho, udp)$) as the width of the multidimensional rectangular region centered around \vec{x} such that with respect to a detector placed at time $t_0 + T$ and spatial position \vec{x} , for each $\vec{p} \in \vec{x} \pm P_w(T, \rho, udp)$ at time $t_0 + \rho$, the protection guarantee holds.

LEMMA B.1. *An error affecting any of the MSB udp bits of a point inside the protected width is detected.*

For a point y_i in Y , if y_i belongs to Y_{udp} and its minimal precision contribution is p_i at the final output, then $p_i \geq udp$. If $y_i \in [\underline{y_i}, \overline{y_i}]$, then an error, err_{y_i} affecting within the MSB udp bits will be bounded by $err_{y_i} \geq 2^{\exp(\underline{y_i}) - p_i + 1}$. Since, we are matching dp bits at the detector, hence the threshold of detectable error is bounded by $2^{\exp(\overline{S_Y}) - dp_T + 1}$. For our guarantee to hold, the following must be true

$$\begin{aligned} \text{generated error} &\geq \text{error threshold} \\ 2^{\exp(\underline{y_i}) - p_i + 1} &\geq 2^{\exp(\overline{S_Y}) - dp_T + 1} \end{aligned} \quad (33)$$

Taking logarithms and simplifying the above terms leads to the following relation that must hold true for all points inside the P_w region.

$$\begin{aligned} \exp(\overline{S_Y}) - \exp(\underline{y}_i) &\leq dp_T - p_i \\ udp \leq p_i &\leq dp_T - \{\exp(\overline{S_Y}) - \exp(\underline{y}_i)\} \end{aligned} \quad (34)$$

In figure 5 , the enclosed region ($\rho \times P_w$) for the given detector location T-steps ahead forms the protected region for that detector. In determining the protected region, where a detector is used to protect iteration points in multiple time steps, we choose ρ such that the protected width chosen at ρ is also valid for all time points $t_0 \leq t \leq t_0 + \rho$:

$$\forall 0 \leq t \leq \rho : P_w(T, \rho, udp) \leq P_w(T, t, udp) \quad (35)$$

B.4 Modeling Essential Width (E_w)

Essential width models the maximum set of points in X absolutely necessary to obtain dp_T precision at the detector location. If the maximal contribution of y_i to the output falls below ulp of the desired precision, then y_i can be safely discarded. Ofcourse, all discarded points collectively could still affect within the required precision. Hence, there is an iterative process to carve out a set of excluded points. To this end, we compare y_i 's maximal contribution with respect to the minimal contribution from all the remaining points. We define $d_{\min}(y_i)$ as the distance between the exponent of the lower bound of $S_{Y \setminus i}$ and the exponent of the upper bound for y_i such that

$$d_{\min}(y_i) = \max(0, \exp(\overline{S_{Y \setminus i}}) - \exp(\underline{y}_i)) \quad (36)$$

The maximal precision contribution of point y_i to the final sum S_Y when S_Y is computed up to p precision bits is

$$\maxContrib_p(y_i, S_Y) = p - d_{\min}(y_i) \quad (37)$$

In our stencil model for detector placed at $A_u[\vec{x}, t_0 + T]$, we define **Essential Width** (E_w) as the width of the multidimensional rectangular region around \vec{x} such that the direct evaluation over E_w is sufficient to guarantee dp_T precision at the detector. Specifically, the region is defined by extents E_{wl} and E_{wr} such that $E_w = E_{wl} + E_{wr} + 1$. Figure 5 illustrates E_w for evaluation of a 1-D stencil over T-steps.

LEMMA B.2. *In the absence of an error, direct evaluation over the essential width (E_w) ensures the correctness of the computation to at least dp_T bits of precision at the detector location.*

For all points in the region excluded from $E_w \forall \tilde{X} : \tilde{X} \subset ([\vec{x} \pm \vec{w}T] - E_w)$, the following holds

$$\forall x_i \in \tilde{X} : \maxContrib_{dp_T} \left(\sum (y_i = c_i \times x_i), S_Y \right) \leq 0 \quad (38)$$

One form of false positives involves detection of soft errors when no error affects any iteration point on which the detector depends (aka the detector's dependence cone). The preceding lemma guarantees that, despite the reduced evaluation cost, in the absence of errors affecting the dependence code, the direct evaluation is equivalent to the iterative evaluation within dp bits and no soft error notification(false alarms) is triggered.

In essence, Essential Width (E_w) provides a method to reduce the detector evaluation cost while retaining the quality of the detector precision (dp_T). The Protected Width (P_w) on the other hand characterizes a detectors maximum reach to provide rigorous protection for an enclosed region of space per detector. Hence, obtaining an optimal combination of (E_w, P_w, ρ) allows *FPDetect* to situate detectors sparsely and effectively over the entire compute space.

C OVERALL ALGORITHM

To efficiently deploy *FPDetect*'s detectors during online execution, we build a look-up table of detector configurations using an offline profiling pass without actually looking at the input data. This allows the detector configurations to be valid for a large range of initialization and boundary constraints when being instantiated online. For each anticipated choice of *udp*, probability of detection, and anticipated input range, the offline analysis determines the detector configuration to be used during online execution. A detector configuration consists of: T , the distance at which the single-direct detector is evaluated; ρ , the number of iterations between certified baselines; E_w , the essential width to evaluate the detector; Detector coefficients for the values in the essential width; and P_w , the spatial separation between detectors in the same time step. These parameters completely specify the detector configuration at runtime.

C.1 Offline algorithm.

We consider all T and ρ such that $T \leq T_{\max}$, $\rho < T$. To constrain the search space of possible configurations, we use a customizable upper bound on the Tstep (say, $T_{\max} = 256$) that one may use for the detector evaluation. Furthermore, having a very large T impacts coverage around the boundary region. For a d -dimensional stencil, P_w is d -dimensional vector, corresponding to protected region of iteration points centered at the detector. E_w is represented by a rectangular region with a computed number of points along left and right of the detector along each direction. These extents along dimension i are denoted by ewl_i and ewr_i with $ew_i = ewl_i + ewr_i + 1$. The cost function for a 5-tuple detector configuration ($exp, udp, T, \rho, Coeffs$) is given as

$$Cost = \frac{1}{\rho} \prod_{i=1}^d \left(\frac{ew_i}{pw_i} \right) \quad (39)$$

Even though the tuple elements exp , T , and $Coeffs$ do not explicitly appear in the cost function, they implicitly influence the cost through E_w and P_w .

```

1  struct Config {
2      double volume, cost;
3      int dt, rho, pwvec, ewlvec, ewrvec;
4  };
5  auto offline_analysis(Tmax, exp_set, udp_set, cov_set) {
6      for exp in exp_set:
7          //compute maxdp[t] for 1<=t<=Tmax
8          //compute ewcost[t] as product of elements of vector ew[exp,t,maxdp[t]]
9          for b in udp_set:
10             COV[nt, nt, wvec] = //number of points in region [dt:dt+rho][-i:i][-j:j] with b bits of coverage
11             for dt = nt-1 .. 0 and rho = nt-dt .. dt+1:
12                 forall ivec:
13                     cost = VOLUME(dt, rho, ivec) / ewcost[dt+rho];
14                 for c in cov_set:
15                     if COV(dt, rho, ivec) >= c && configs[exp,b,c].cost < cost
16                         configs[exp,b,c] = {vol, cost, dt, rho, ivec, ewl[dt+rho], ewr[dt+rho]}
17             return configs;
18  }
```

Fig. 6. Offline profiler for optimal detector configurations

Figure 6 outlines the steps involved in the offline analysis. The algorithm takes as input parameters for which offline profiles need to be determined: the maximum number of time steps (T_{\max}), the set of input ranges (as exponents in exp_set), set of *udp* values (as udp_set), and probabilistic coverage values (cov_set). The algorithm determines the configurations one input range choice at a time.

Using floating-point round-off analysis, the maximum number of bits that will be preserved for each possible time step t is computed (as maxdp). For each t , the cost of evaluating each detector is computed as the product of the $e\vec{w}$ dimensions to guarantee $\text{maxdp}[t]$ bits of precision of the direct evaluation t time steps away. Then, for each candidate protected region, the fraction of points with guaranteed coverage of b bits (where b is a candidate udp in the input parameter udp_set) is computed. If this fraction is greater than a desired coverage and if the associated cost is lower than that of any configuration seen thus far, this configuration is chosen. After evaluating all feasible solutions, the algorithm returns the last chosen configurations.

Algorithm 1 Online Detection

```

1: function ONLINEDETECTION( $A=\text{Stencil}, \text{udp}, \text{cov}$ )
2:    $I = \text{ScanInput}(A)$ 
3:    $\text{exp} = \text{MapInterval}(I)$ 
4:    $\text{in\_cov} = \text{AdjustCoverage}(\text{cov})$ 
5:    $\{T, \rho, dp, \vec{E}_w, \vec{P}_w\} = \text{lookup\_configuration}[(\text{exp}, \text{udp}, \text{in\_cov})]$ 
6:    $\text{Coeffs} = \text{get\_coefficient}(\text{Stencil}, T, \vec{E}_w)$ 
7:    $\text{configure\_detectors}(\{T, \rho, dp, \vec{E}_w, \vec{P}_w\})$ 
8:    $\text{cur} = 0; t_\delta = T - \rho$ 
9:    $D[0] = \text{eval\_detector}(A, \text{Coeffs})$ 
10:   $\text{execute\_stencil}(\min(\text{ITER}, \rho), A)$ 
11:  for  $t = \rho; t < \text{ITER}; t += \rho$  do
12:     $\text{cur} = 1 - \text{cur}$ 
13:     $D[\text{cur}] = \text{eval\_detector}(A, \text{Coeffs})$ 
14:     $\text{execute\_stencil}(\min(\text{ITER}-t, t_\delta), A)$ 
15:    if  $t + t_\delta \leq \text{ITER}$  then
16:       $\text{detector\_check}(A, D[1 - \text{cur}])$ 
17:    if  $t + t_\delta < \text{ITER}$  then
18:       $\text{execute\_stencil}(\min(\text{ITER}-(t + T - \rho), \rho - t_\delta))$ 
19:  if  $\text{ITER} > \rho$  and  $\text{ITER} \% \rho < t_\delta$  then
20:     $\text{trailing\_detector}(D[1 - \text{cur}], A)$ 
21:  if  $\text{ITER} \% \rho \neq 0$  then
22:     $\text{trailing\_detector}(D[\text{cur}], A)$ 

```

C.2 Online Detector-Embedded Execution

Algorithm 1 outlines the online detector-embedded execution of a given stencil kernel. The input values are scanned to compute the input exponent range to be handled in the floating-point space (lines 2–3). To account for the unprotected boundary regions, user’s input cov value is mapped to an equivalent internal coverage value (in_cov) that corresponds to the detection probability on the grid excluding the boundaries. The adjustment is done with the guarantee that the fraction of points covered due to (in_cov) is at least as many required by cov over the entire computation space. If an equivalent mapping is not found by (AdjustedCoverage), the program exits conveying an error message for unsupported coverage. The input range, the user-specified udp , and the modified detection probability (in_cov) are used to lookup the detector configuration (lines 5–7).

After an initial evaluation of the detector and the stencil for ρ iterations (lines 9–10), the execution of the stencil (execute_stencil) is split into two segments: iterations till the next detector evaluation (eval_detector and iterations till the next detector check (detector_check). Thus, the stencil is executed with interleaved detector evaluation and checking (lines 11–18). Note that the algorithm assumes ρ is greater than half the detector evaluation T -step. This scenario requires at most two “live”, i.e., unchecked detectors per spatial position in the iteration space, at any time. If not, at each spatial position, multiple detectors need to be evaluated and retained until they are checked.

When all iterations of the stencil have been executed, the iterations past the last certified baseline need to be checked. To protect any leftover iterations, the computation since the last certified baseline is checked using the trailing detection strategy (lines 19–22).

D SOFTWARE BUG DETECTION

FPDetect's evaluation units can be efficiently utilized to trap logical and compiler transformation (polyhedral transforms exploiting data locality and parallelism) induced bugs. The design of these evaluation units model the actual stencil in real equivalent space and hence are logically equivalent to the actual stencil without any modeling bias. Thus any transformation bugs introduced into the stencil codes later through optimization will result in mismatch with our evaluation units. Hypothesizing that such bugs lead to systematic errors impacting floating point values non-trivially, we intend to trap bugs in the floating point space within a precision threshold. As such, there remains possibility that bugs escape beyond the threshold we check for (controlled by the detector precision).

Table 2. Summary of Pluto generated code.

Benchmarks	SLOC spec	SLOC Pluto	Num Loops	Nesting Level
H1	27	905	374	7
H2	52	1164	370	7
H3	65	905	374	11
H4	54	2314	486	6
H5	54	2314	486	6
H6	54	2314	486	6
P1	23	31	12	6
P2	23	31	12	6
P3	19	31	12	6
P4	63	1163	370	6
P5	39	1163	370	6
P6	39	1163	370	6
P7	47	1165	414	6
P8	47	956	416	6
P9	47	956	416	6
W1	70	1157	360	6
W2	70	1157	360	6
W3	70	1157	360	6
W4	70	1157	360	6
W5	70	1157	360	6
W6	70	1157	360	6
C1	53	1157	360	6
C2	53	1157	360	6
C3	53	1157	360	6

Summary of Pluto generated code: We studied the effectiveness of *FPDetect*'s evaluation units in bugs introduced to evaluate polycheck [2] on Pluto [3] optimized stencil codes. To generate optimized versions using Pluto, we implemented all the stencils in the form of affine loop nests enclosed in scop pragmas. This code input to Pluto has consists of median 53 source lines of code (SLOC)² per benchmark. Pluto takes these scop-annotated benchmarks as input to generate optimized versions with median 1157 SLOC. The median of the number of loops in the transformed code was 365 across all the benchmarks with a median nesting depth of 6. In checking such large and complex generated codes, tools such as *FPDetect* are essential. Table 2 provides a summary of the Pluto generated code. The 'spec' refers the original stencil code prior to feeding into Pluto.

²Source lines of code are measured using sloccount tool

We report the source lines of code (SLOC) for both the ‘spec’ and the Pluto optimized version alongwith the number of loops and nesting levels in the transformed code. The number of loops and nesting levels drive the complexity of the tests being performed since each ‘for loop’ entry point becomes a potential bug-injection site.

The bugs introduced in the source potentially affect multiple runtime operations making them easier to detect. These tests fall under three categories based on the generated errors impacting: (1)*Loop bounds*, resulting in an incorrect stencil pattern at the tile boundaries, (2)*array access*, affecting the stencil footprint used, and (3)*Loop reordering*, affecting the data dependencies. We discuss each of them with an example as discussed below.

Loop Bounds: To inject errors impacting ‘loop’ bounds, we first identified all the ‘for’ loop sites present in the transformed code. Error injection was performed by either adding one to a lower bound of a for loop or subtracting one from an upper bound. This was automated by replacing each bound, x , for an identified ‘for loop’ with a call to a function **bound**(c, x) where c is a constant integer number identifying each unique callsite and x is the actual bound in the original ‘for loop’ of the transformed code as shown in figure 7.

```

1 for (t1=-938)t1<=floord(3*steps,32);t1++) {
2   for (t2=lbp;t2<=ubp;t2++) {
1   for (t1= bound (0, -938);t1<= bound (1, floord(3*steps,32));t1++) {
2     for (t2= bound (2, lbp);t2<= bound (3, ubp);t2++) {

```

Fig. 7. Source code before and after bound replacement

A callsite can be selected by command line argument and the resulting execution will have the indicated bound changed. The **bound** function returns the x value (the original bound) if the callsite does not match the selected callsite for fault injection. If it is the selected call-site, then it return $x + 1$ if c is even or $x - 1$ if c is odd.

Array Access: Similarly the array access errors were injected using a function utilizing a unique integer. Each ‘for’ loop site was replace by the function **acs** with a unique integer ID as shown in the figure 8. On encountering an **acs** function call, it returns the original access value if its unique ID number do not match the intended injection call site ID. for injection. When it matches, it returns the modiefied the access value by dividing it by two.

```

1 A[ ((32*t1+15056)/3) - 1) % 2][10000][((-32*t1+3*t6-15056)/3)]
1 A[ acs (51, ((32*t1+15056)/3) - 1) % 2][ acs (52, 10000)][ acs (53, ((-32*t1+3*t6-15056)/3))]

```

Fig. 8. Source code before and after access replacement

For both these methods of automatic injection there are three counts that come about. One is the number of source code locations modified. Another is the number of locations reached by the running code. The final number is the number of locations reached which actually changed the computation. Not all source locations where an error can be injected are reachable at run time. Table 3 identifies the source locations (#*SL*) identified and the number of runtime locations (#*RL*) actually reached for injecting a bug. For example, in benchmark H4, there are 486 locations for injecting a bug that can potentially impact a loop-bound, however only 106 of them are reached at runtime.

False positives. Some bugs do not result in any difference in our bitwise comparison of the result with the non-buggy version. Therefore, our approach incurs no false positives in our evaluation. This is because some source-level bugs do not manifest at runtime. For example, a loop iterator

might be constrained by multiple loop bounds (e.g., min or max of multiple expressions), with the loop bound never reaching the error-injected expressions. For example, in benchmark H4, there are 486 locations for injecting a bug that can potentially impact a loop-bound, however only 106 of them are reached at runtime. Figure 9 lists an example where the ‘for’ loop iterator passes through two nested ‘if’ checks that can potentially mask an error in the iterator due to a bug impacting the ‘for loop’ bound value.

```

1  for (t1=-938; t1<value; t1++) {
2    if (2*t1%3 == 0) {
3      if ((t1+3)%6 == 0) {
4        <body>
5      }
6    }
7  }

```

Fig. 9. An example of nested if statements in Pluto transformed code

Table 3 summarizes *FPDetect*’s bug detection effectiveness for the above two categories of bugs. The table only lists detection percentages when the bitwise comparison with the non-buggy version flags an error-injected version as being in error.

Table 3. Software bug detection results.

	Loop bound			Array access			Loop bound			Array access			
	#SL	#RL	%det	#Sl	#Rl	%det	#SL	#RL	%det	#Sl	#Rl	%det	
H1	374	374	100	300	267	99.67	H2	370	370	100	300	258	100
H3	374	374	100	300	267	98	H4	486	106	99.79	300	26	100
H5	486	106	100	300	26	100	H6	486	106	100	300	26	100
P1	10	10	100	18	17	100	P2	12	12	100	18	17	100
P3	12	12	100	18	17	100	P4	370	310	100	300	223	87.67
P5	370	310	96.22	300	223	82.67	P6	370	310	96.22	300	223	82.33
P7	414	104	98.55	300	48	97	P8	416	104	100	300	44	98.67
P9	416	104	98.56	300	44	98	W1	360	280	100	300	215	55.33
W2	360	280	44.72	11	6	54.67	W3	360	350	31.11	300	266	45.33
W4	260	280	45.28	300	215	60	W5	360	280	53.61	300	215	62.67
W6	360	350	100	300	266	100	C1	360	360	100	300	262	100
C2	360	360	100	300	262	100	C3	360	360	100	300	262	100

Loop ordering: Loop reordering was performed by hand. Figure 10 contains an example of loop reordering where the first two loops are swapped. Changing the order of updates to *A* substantially changed the result of the computation.

Unlike changes to array accesses and loop bounds, changing loop orders required non-local changes to the Pluto-generated code. Therefore, we handcrafted the error injected versions. The handcrafted scenarios included swapping nested loop pairs and re-ordering of non-nested loop blocks. The optimized codes included a maximum of 360 nested for loops with a maximum loop nesting depth of 11. Testing all possible combinations of loop reorderings will be prohibitively expensive. We limited our testing to 15 loop order bug injections per benchmark. Figure 10 contains an example of loop reordering where the first two loops are swapped.

```

1  for (t4=max(1,ceild(16*t1+48*t2+48*t3,3));
2      t4<=min(min(min(min(floord(16*t1+48*t2+48*t3+141,3),steps),64*t2-1),64*t3-1),16*t1-16*t2-16*t3+9999);
3      t4++) {
4      for (t5=max(64*t2,-16*t1+16*t2-48*t3+3*t4-78);t5<=min(64*t2+63,-16*t1+16*t2-48*t3+3*t4);t5++) {
5          lbv=max(64*t3,-16*t1+16*t2+16*t3+3*t4-t5-15);
6          ubv=min(64*t3+63,-16*t1+16*t2+16*t3+3*t4-t5);
7          for (t6=lbv;t6<=ubv;t6++) {
8              A[(t4-1)%2][(-t4+t5)][(-t4+t6)] = (((((0.5 * A[t4%2][(-t4+t5)][(-t4+t6)])) + ...
9              )
10             )
11             }
12         }
13     }

1  for (t5=max(64*t2,-16*t1+16*t2-48*t3+3*t4-78);t5<=min(64*t2+63,-16*t1+16*t2-48*t3+3*t4);t5++) {
2      for (t4=max(1,ceild(16*t1+48*t2+48*t3,3));
3          t4<=min(min(min(min(floord(16*t1+48*t2+48*t3+141,3),steps),64*t2-1),64*t3-1),16*t1-16*t2-16*t3+9999);
4          t4++) {
5          lbv=max(64*t3,-16*t1+16*t2+16*t3+3*t4-t5-15);
6          ubv=min(64*t3+63,-16*t1+16*t2+16*t3+3*t4-t5);
7          for (t6=lbv;t6<=ubv;t6++) {
8              A[(t4-1)%2][(-t4+t5)][(-t4+t6)] = (((((0.5 * A[t4%2][(-t4+t5)][(-t4+t6)])) + ...
9              )
10             )
11             }
12         }
13     }

```

Fig. 10. Source code before and after manual loop reordering

REFERENCES

- [1] 2008. IEEE Standard for Floating-Point Arithmetic. *IEEE Std 754-2008* (Aug 2008), 1–70. <https://doi.org/10.1109/IEEESTD.2008.4610935>
- [2] Wenlei Bao, Sriram Krishnamoorthy, Louis-Noël Pouchet, Fabrice Rastello, and P. Sadayappan. 2016. PolyCheck: dynamic verification of iteration space transformations on affine programs. In *POPL*. 539–554.
- [3] Uday Bondhugula, Muthu Baskaran, Sriram Krishnamoorthy, J. Ramanujam, A. Rountev, and P. Sadayappan. 2008. Automatic Transformations for Communication-Minimized Parallelization and Locality Optimization in the Polyhedral Model. In *ETAPS CC*.
- [4] Eva Darulova and Viktor Kuncak. 2017. Towards a Compiler for Reals. *ACM Trans. Program. Lang. Syst.* 39, 2, Article 8 (March 2017), 28 pages.
- [5] Luiz Henrique de Figueiredo and Jorge Stolfi. 2004. Affine Arithmetic: Concepts and Applications. *Numerical Algorithms* 37, 1 (01 Dec 2004), 147–158.
- [6] William Kahan. 1996. IEEE standard 754 for binary floating-point arithmetic. *Lecture Notes on the Status of IEEE 754*, 94720-1776 (1996), 11.